ELEMENTA
Science of the Anthropocene

Matrosov, SY, et al. 2022. High temporal resolution estimates of Arctic snowfall rates emphasizing gauge and radar-based retrievals from the MOSAiC expedition. *Elem Sci Anth*, 10: 1. DOI: https://doi.org/10.1525/elementa.2021.00101

RESEARCH ARTICLE

High temporal resolution estimates of Arctic snowfall rates emphasizing gauge and radar-based retrievals from the MOSAiC expedition

Sergey Y. Matrosov[1,2,*], Matthew D. Shupe[1,2], and Taneil Uttal[2]

This article presents the results of snowfall rate and accumulation estimates from a vertically pointing 35-GHz radar and other sensors deployed during the Multidisciplinary drifting Observatory for the Study of Arctic Climate (MOSAiC) expedition. The radar-based retrievals are the most consistent in terms of data availability and are largely immune to blowing snow. The total liquid-equivalent accumulation during the snow accumulation season is around 110 mm, with more abundant precipitation during spring months. About half of the total accumulation came from weak snowfall with rates less than approximately 0.2 mmh^{-1}. The total snowfall estimates from a Vaisala optical sensor aboard the icebreaker are similar to those from radar retrievals, though their daily and monthly accumulations and instantaneous rates varied significantly. Compared to radar retrievals and the icebreaker optical sensor data, measurements from an identical optical sensor at an ice camp are biased high. Blowing snow effects, in part, explain differences. Weighing gauge measurements significantly overestimate snowfall during February–April 2020 as compared to other sensors and are not well suited for estimating instantaneous snowfall rates. The icebreaker optical disdrometer estimates of snowfall rates are, on average, relatively little biased compared to radar retrievals when raw particle counts are available and appropriate snowflake mass-size relations are used. These counts, however, are not available during periods that produced more than a third of the total snowfall. While there are uncertainties in the radar-based retrievals due to the choice of reflectivity-snowfall rate relations, the major error contributor is the uncertainty in the radar absolute calibration. The MOSAiC radar calibration is evaluated using comparisons with other radars and liquid water cloud–drizzle processes observed during summer. Overall, this study describes a consistent, radar-based snowfall rate product for MOSAiC that provides significant insight into Central Arctic snowfall and can be used for many other purposes.

Keywords: MOSAiC, Cloud radar, Snowfall

1. Introduction

Snowfall is a crucial element of the Arctic climate system. It affects thermodynamic profiles in the atmosphere through latent heat transfers associated with snowfall processes (e.g., water vapor deposition, sublimation). Snowfall is one of the largest sinks of moisture in the atmosphere, and it is also a significant component of the Earth's hydrological cycle. Snow on the surface, which is generally determined by snowfall, affects the albedo and the thermal conduction of energy through the subsurface layer, thus playing important roles in the surface energy budget. Because of these processes, quantifying snow layers on sea ice is also important for sea-ice forecasts (Webster et al., 2020; Wagner et al., 2021).

Some satellite measurements, such as those from the *CloudSat* W-band (approximately 94 GHz) spaceborne profiling radar (Im et al., 2005; Wood et al., 2013), provide retrievals of mean snowfall rates that are in reasonable agreement with estimates from the ground-based U.S. Weather Surveillance Radar-1988 Doppler (WSR-88D) network (Matrosov, 2019). These satellite measurements, however, are limited to the areas that are approximately south of the 82° Northern latitude, thus missing a significant portion of the central Arctic Ocean. In situ measurements of snowfall in the central Arctic Ocean are extremely scarce, especially in the winter months. As remote sensing measurements, ground-based measurements of snowfall usually have large uncertainties (Rasmussen et al., 2012).

The Multidisciplinary drifting Observatory for the Study of Arctic Climate (MOSAiC) expedition was a 1-yearlong field experiment in the Central Arctic, which started in

[1] Cooperative Institute for Research in Environmental Sciences, University of Colorado, Boulder, CO, USA

[2] National Atmospheric and Oceanic Administration, Physical Sciences Laboratory, Boulder, CO, USA

* Corresponding author:
Email: sergey.matrosov@noaa.gov

early October 2019. The overarching goal of the expedition was to collect a comprehensive data set about the Arctic climate system in an area that is undergoing fast changes and generally lacks reliable observations of many components of this system (Shupe et al., 2020). Many remote and in situ sensors were deployed onboard the drifting icebreaker Polarstern and in a nearby sea-ice camp to make measurements of atmospheric, oceanic, and sea-ice properties that affect the climate system (Shupe et al., 2022). These measurements will be used to refine existing, and develop new, regional and global climate models. Such models can serve as tools to understand climate change and enhance weather and sea-ice forecasts in the Arctic region where model uncertainties are among the largest (Hodson et al., 2013).

A remote sensing instrumentation suite on the icebreaker, included a Department of Energy (DOE) Atmospheric Radiation Measurement (ARM) Program K_a-band (approximately 35 GHz) zenith-pointing radar (KAZR). Although originally designed for cloud observations (Kropfli et al., 1990), millimeter-wavelength radars operating at K_a- and W-bands have also proved to be very useful for snowfall measurements (Matrosov et al., 2008). A ground-based K_a-band radar similar to the KAZR was first used for snowfall retrievals during the Surface Heat Budget of the Arctic Ocean study (Uttal et al., 2002), where radar-derived accumulations were on average biased high by 23% compared to the surface snowfall gauge measurements (Matrosov et al., 2008).

Cloud radar–based observations used to derive snowfall are usually obtained from the lowest sufficiently reliable range gate (i.e., at a height of 160 m from the radar site, which was at 14 m above the surface during MOSAiC), which alleviates effects of blowing snow on radar echoes. The radar-based approach can provide high-temporal resolution estimates of instantaneous snowfall rate (i.e., snowfall flux) unlike tipping bucket-type gauge data, which are based on incremental "tip" measurements. High-temporal resolution snowfall data are needed for many practical applications including model verification.

The objectives of this study were (1) to assess the consistency of various snowfall measurements using different approaches and MOSAiC precipitation sensors/gauges with an emphasis on evaluating the quality of radar-based snowfall estimates, (2) to quantify the seasonal evolution of snowfall at MOSAiC, and (3) to derive a consistent MOSAiC data set of high temporal resolution (approximately 30 s) snowfall rate/flux data that can enable further model and observational studies of snowfall and its processes.

2. Radar-based snowfall retrieval approach

The KAZR-type radars used in this study are deployed at most of the fixed ARM sites and mobile facilities worldwide. ARM's North Slope of Alaska (NSA) facility (71.325° N, 156.608° W) is a convenient location for testing and verification of KAZR-based retrievals of snowfall rates. Importantly, a National Oceanic and Atmospheric Administration (NOAA) U.S. Climate Reference Network (CRN) station (Diamond et al., 2013) is located next to the NSA ARM facility at Utqiaġvik (formerly Barrow, Alaska). It operates a Geonor-type (Lamb and Swenson 2005) weighing precipitation gauge with a double fence intercomparison reference (DFIR) wind shield. This type of DFIR gauge serves as a World Meteorological Organization standard reference for measuring solid precipitation and is considered to provide the most reliable estimates of snowfall accumulations (Rasmussen et al., 2012).

The absolute calibration of the NSA KAZR radar in the general (GE) measurement mode has been recently evaluated using drizzle-cloud microphysical processes (Maahn et al., 2019). This evaluation indicated that the NSA KAZR equivalent reflectivity factors (Z_e, hereafter reflectivities) were about 1 dB too low, but this average offset was stable in time. Statistical comparisons of KAZR and *CloudSat* measurements for an earlier period suggested a bias of about 3 dB (Kollias et al., 2019). The absolute calibration of observed Z_e values is important, since for vertically pointing radars, snowfall retrievals are primarily based on relations between Z_e and liquid-equivalent snowfall rate, S, that are typically expressed as a power-law approximation:

$$Z_e(\mathrm{mm^6 m^{-3}}) = a\, S^b(\mathrm{mm\ h^{-1}}), \qquad (1)$$

where a and b are obtained either theoretically or empirically. Reflectivities for vertically pointing radar measurements (especially those at cloud radar frequencies) depend on the degree of particle nonsphericity (Matrosov et al., 2012). One of the earliest K_a-band, Z_e–S relations was suggested by Matrosov (2007). The mean values of coefficients a and b (56 and 1.2, respectively) for typical atmospheric pressure (approximately 1013 hPa) were obtained assuming that the average aspect ratio of ice hydrometeors (i.e., the ratio of particle minor and major dimensions) is 0.6. This average value was obtained from two-dimensional particle projections in an in situ aircraft-based observational study of Korolev and Isaac (2003). Advanced polarimetric radar measurements can provide information on precipitation type and general shape of both solid and liquid hydrometeors (Reinking et al., 2002; Matrosov et al., 2012; Matrosov, 2021). MOSAiC cloud radars, however, were measuring only a single polarimetric variable—linear depolarization ratio (LDR), which is strongly affected by particle orientation and is not ideal for hydrometeor shape retrievals.

Recent retrievals of snowflake shapes near the ground using advanced scanning polarimetric radar measurements at Oliktok Point, Alaska, have indicated that their mean aspect ratio is often between 0.4 and 0.6 (Matrosov et al., 2020). The use of the microphysical data set from Matrosov (2007) with a change of the assumption about the average snowflake aspect ratio (i.e., 0.5 instead of 0.6) results in Equation 1 coefficient a and b values of approximately 63 and 1.2. Thus, the relation $Z_e\,(\mathrm{mm^6 m^{-3}}) = 63\, S^{1.2}$ ($\mathrm{mm\ h^{-1}}$) was used here for snowfall rate retrievals. **Figure 1** compares relations $Z_e = 63\, S^{1.2}$ and $Z_e = 56\, S^{1.2}$ with several other K_a-band Z_e–S relations obtained empirically using observational data (e.g., Falconi et al., 2018; Heymsfield et al., 2018; Huang et al., 2019) for different

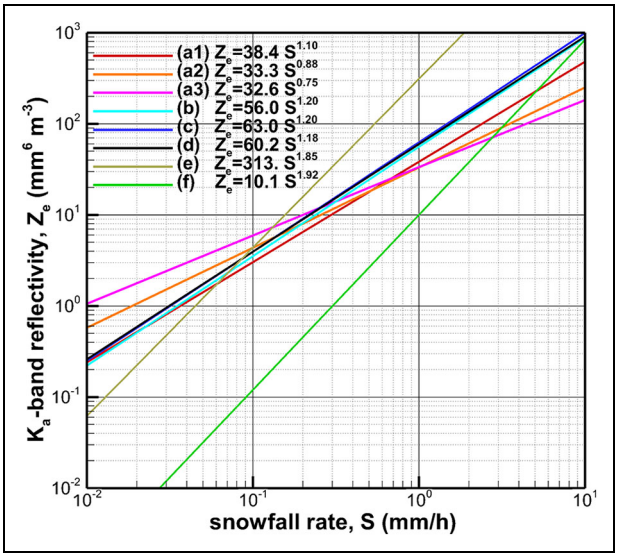

Figure 1. Standard air pressure K_a-band Z_e–S relations for vertically pointing radar measurements from different studies: (a1), (a2), and (a3) Falconi et al.'s (2018) relations for low, moderate, and high rime snow, correspondingly, and their table 2, (b) Matrosov (2007), (c) this study, (d) Huang et al. (2019) and their table 3 HB method producing the best agreement with gauge data, (e) Kulie and Bennartz (2009) for aggregate snowflakes, and (f) Heymsfield et al. (2018) and their table 3. DOI: https://doi.org/10.1525/elementa.2021.00101.f1

snow conditions and also theoretical considerations (e.g., Kulie and Bennartz, 2009). It is clear that this set of relationships produces a wide range of snowfall rates as a function of reflectivity, implying significant uncertainties in these relationships.

The relation $Z_e = 63\ S^{1.2}$ was applied to the NSA KAZR measurements to retrieve snowfall rates during a 6-month cold season period (November 1, 2017, to April 30, 2018) when practically all observed precipitation fell as snowfall. KAZR reflectivities were corrected for the 1-dB mean offset as found by Maahn et al. (2019). **Figure 2** shows time series of the liquid-equivalent snowfall accumulation for the radar-based retrieval. The snowfall rate retrieval was applied to radar measurements with a time resolution of about 3.7s and then averaged in 1-min intervals. The lowest radar range gate used for the retrieval was at a height of 0.16 km above the KAZR location, which is high enough to minimize the effects of blowing snow near the ground. Attenuation of the K_a-band radar signal in atmospheric gases and dry snow at shorter ranges is generally small compared to the radar calibration uncertainties and was neglected. Since particle terminal velocities are approximately scaled as $\rho_a^{-0.43}$, (Pruppacher and Klett, 1978), where ρ_a is the air density, the snowfall rate inferred from Equation 1 was corrected using a mean vertical profile of air density to get an estimate at a height h as:

$$S(h) = S[\rho_a(h=0)/\rho_a(h)]^{0.43}. \quad (2)$$

For comparison, equivalent melted snowfall accumulation from the CRN DFIR gauge and a collocated Vaisala Present Weather Detector (PWD) optical precipitation sensor are also shown in **Figure 2a**. The CRN and PWD data are sampled at 5- and 1-min time intervals, respectively. The NSA Vaisala PWD system is similar to the PWD systems deployed at MOSAiC (see Section 3). **Figure 2a** shows that the agreement between CRN gauge data and radar retrievals of total snowfall accumulation for the entire 6-month period is relatively good, even though some noticeable differences exist at particular times.

To illustrate these differences, **Figure 2b** shows a scatter plot of CRN (a_{CRN}) and KAZR (a_{KAZR}) derived 24-h accumulations for snowfall days. It can be seen that a number of very small accumulations (<0.01 mm) retrieved by the radar were not recorded by the CRN gauge. For the data in **Figure 2a**, the normalized bias (NB), which is a statistical metric often used when comparing radar-based retrievals with gauges (defined as NB = $<(a_{KAZR} - a_{CRN})>/<a_{CRN}>100\%$, where the angle brackets denote averaging), is about −13%, and the normalized mean absolute difference (NMAD), which is another statistical metric describing a relative spread of the data (NMAD = $< |a_{KAZR}\text{-}a_{CRN}|>/<a_{CRN}>100\%$), is 79%, respectively. There is also a height dependence of radar-based retrievals indicating that snowfall rate/flux changes as a function of altitude. A collocated PWD sensor consistently overestimated accumulations relative to CRN and radar-based retrievals (**Figure 2a**).

While snow accumulation is an important climatological quantity, many practical and scientific applications (e.g., model verification activities) require knowledge of instantaneous snowfall rates/fluxes. The CRN DFIR gauge, which provides an overall robust reference for accumulation measurements, is not very suitable for the estimates of instantaneous precipitation rates. The shortest time interval of CRN gauge data is 5 min, and the smallest accumulation increment is 0.1 mm. Quite often, however, multiple minimal accumulation increments are recorded at a particular moment in time. Due to issues mentioned above, nonzero snowfall rate data from CRN DFIR weighing gauge are intermittent and can overestimate actual rates at certain times. This is illustrated in **Figure 3**, where estimates of snowfall rate from different sources are shown for an NSA precipitation event observed on January 28, 2018. Note that the first 0.2-mm CRN accumulation increment (at around 01:05 UTC in **Figure 3**) is due to snowfall observed during the previous day.

Unlike the CRN DFIR gauge, the PWD optical sensor and radar retrieval provide continuous, high-temporal resolution instantaneous snowfall rate. The PWD data, however, significantly overestimated snowfall accumulations relative to the CRN reference. Blowing snow probably contributed to the PWD data overestimation. To illustrate this point, **Figure 3b** shows a scatter plot of the difference between PWD and KAZR-based snowfall rates (i.e., $\Delta S = S_{PWD}\text{-}S_{KAZR}$) as a function of near-surface wind speed. A time lag of 160s between KAZR and PWD estimates was

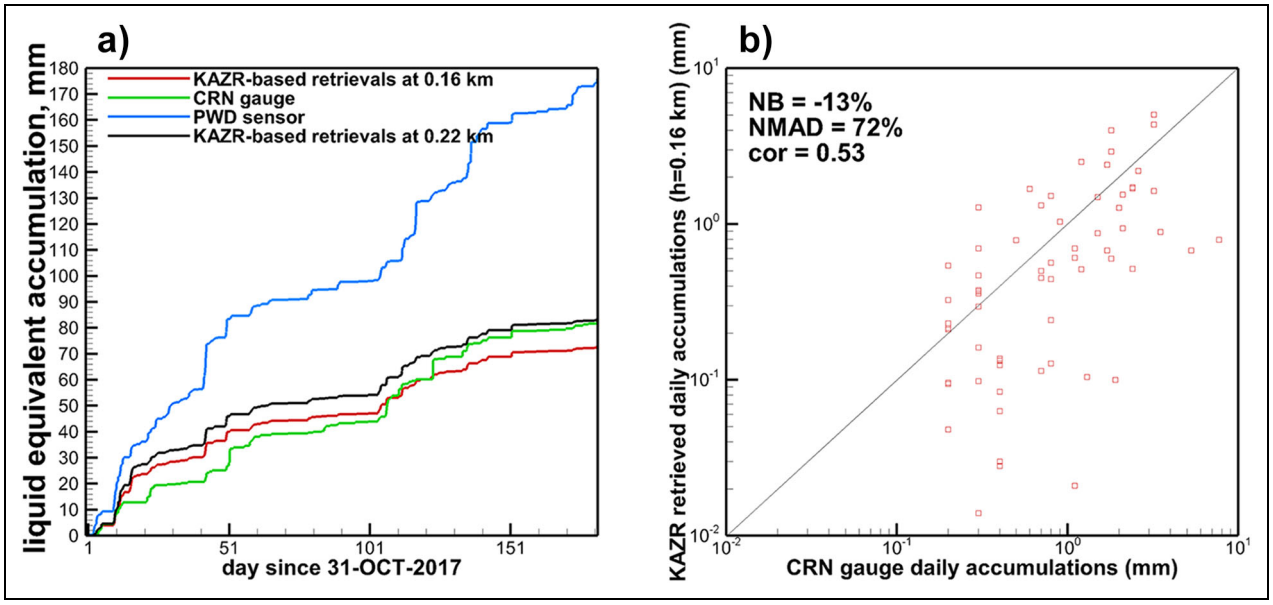

Figure 2. (a) Snowfall accumulation at the North Slope of Alaska site during a 6-month period (November 1, 2017, to April 30, 2018) as retrieved from K_a-band zenith-pointing radar (KAZR) observations at 0.16 km and measured by the Climate Reference Network (CRN) gauge and Vaisala Present Weather Detector optical sensor and (b) a scatterplot of daily accumulations as inferred from the CRN and KAZR measurements. DOI: https://doi.org/10.1525/elementa.2021.00101.f2

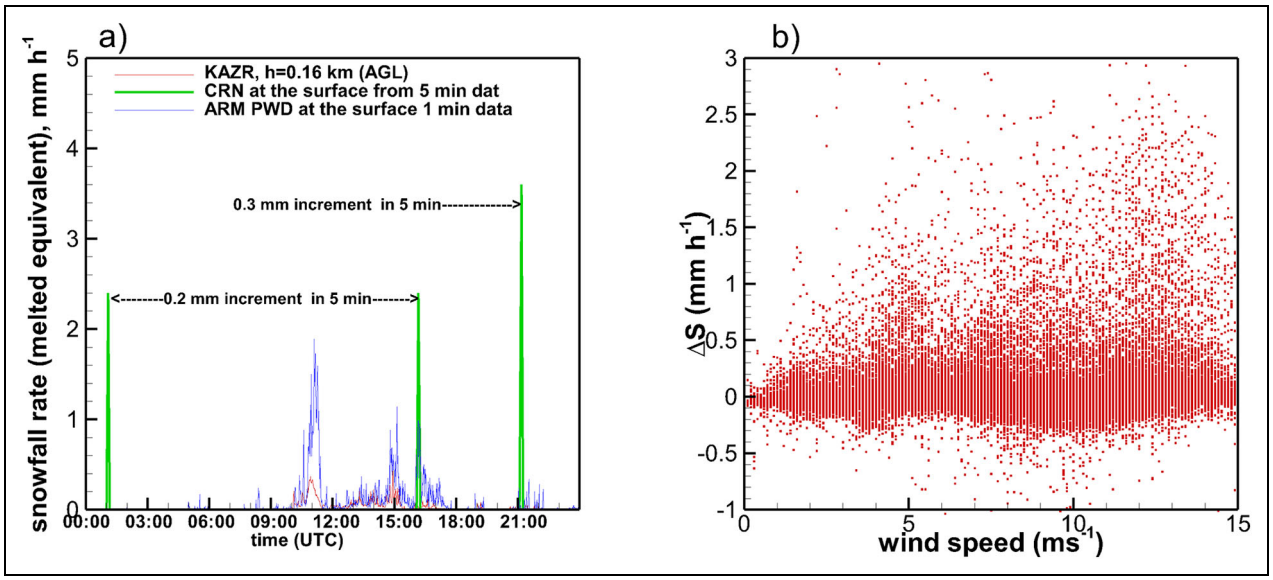

Figure 3. (a) Estimates of snowfall rates at the North Slope of Alaska site from K_a-band zenith-pointing radar (KAZR) retrievals and Climate Reference Network (CRN) gauge and Present Weather Detector sensor data for January 28, 2018, and (b) a scatter plot of the difference between the CRN and KAZR 1-min resolution estimates of snowfall rate as a function of near surface wind speed. DOI: https://doi.org/10.1525/elementa.2021.00101.f3

used to account for a time it takes for snow to reach the ground from 160 m height at typical snowflake fall velocity of 1 ms^{-1}. As seen from **Figure 3b**, ΔS values are generally higher for wind speeds greater than about 3–4 ms^{-1} compared to calm conditions. Radar retrievals provide instantaneous snowfall rate estimates that are in a better agreement with CRN gauge accumulations (**Figure 2a**). This demonstrates the practical utility of KAZR-based retrievals for providing a reliable snowfall data set.

3. MOSAiC snowfall measurements

3.1. MOSAiC snow sensors and gauges

Several snowfall gauges and sensors were deployed during the MOSAiC expedition by the U.S. DOE's ARM Program (Shupe et al., 2022). Two optical sensors, which are parts of the version 22 Vaisala PWD systems (Kyrouac and Holdridge, 2019), were deployed on the icebreaker and in the ice camp, located approximately 400 m away from the icebreaker. Second generation Particle Size and Velocity

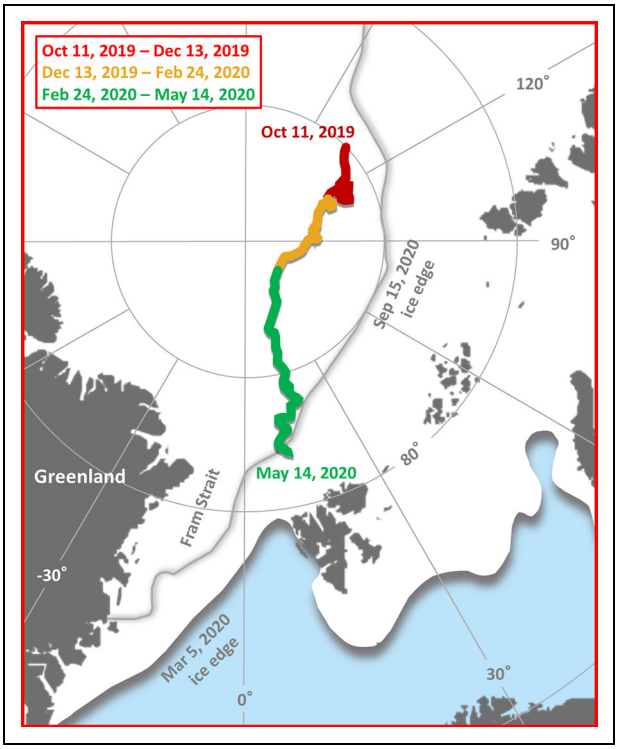

Figure 4. Multidisciplinary drifting Observatory for the Study of Arctic Climate (MOSAiC) expedition track when K_a-band zenith-pointing radar-based snowfall rate retrievals are available. Red, yellow, and green colors correspond to the periods of Legs 1–3 of the MOSAiC expedition, respectively. DOI: https://doi.org/10.1525/elementa.2021.00101.f4

(PARSIVEL-2) optical disdrometers (Nemeth and Beck, 2011; Wang et al., 2019) were also deployed both onboard the icebreaker and in the ice camp. Besides the optical sensors, the ice camp site had a Pluvio weighing bucket precipitation gauge (Nemeth, 2008; Bartholomew, 2020). Additionally, a Siphon gauge and a precipitation sensor, which was a part of the Aerosol Observing System (AOS; Kyrouac and Springston, 2019), were deployed on the icebreaker. To reduce the influences of blowing snow, the ice camp disdrometer and Pluvio gauge were sheltered by double Alter wind shields (Rasmussen et al., 2012).

3.2. Daily accumulations

The KAZR was operational almost continuously during the first MOSAiC drifting period spanning from October 11, 2019, until May 14, 2020. The geographical coordinates of the MOSAiC icebreaker during the drift are shown in **Figure 4**. Some other precipitation sensors became operational at later dates (e.g., starting on October 14 or 17, 2019). There was, however, little precipitation during the period between October 11 and 17, 2019. The radar-based estimates of liquid-equivalent accumulation during the period October 11–17, 2019, were approximately 0.4 mm. During the drift, there were only relatively minor periods when the radar was not operational (most notably a period between approximately 18:40 UTC on March 9, 2020 and approximately 14:20 UTC on March 10, 2020). Near-surface air temperature during the October 2019–May 2020 KAZR operation period was generally below 0°C, so it was assumed that all precipitation fell as snowfall. Some exceptions happened during short periods on April 28 and 29, 2020, when episodes of freezing drizzle were observed. Radar-based retrievals for the entire April 28–29 period, however, indicated only a minor contribution of about 0.2 mm of liquid-equivalent accumulation. GE-mode KAZR measurements (Lindenmaier et al., 2019) were used in this study for snowfall retrievals.

According to the radar-based retrievals using the $Z_e = 63S^{1.2}$ relation, there were 35 instances of daily snowfall accumulations exceeding 1 mm of liquid-equivalent during the October 11, 2019–May 14, 2020, MOSAiC drift period. **Figure 5** shows the time series of the daily accumulations as derived from different MOSAiC sensors. Obvious spurious data from the Pluvio and PWD sensors (e.g., isolated data points indicating liquid-equivalent snowfall rates greater than 10 mm h^{-1} and repetitive data points) were filtered out.

As seen from **Figure 5**, there were several periods of increased precipitation during the drift. Even though the magnitudes of accumulation differ, all the sensors indicate that the highest amount of 24-h snowfall was recorded on April 20, 2020 (day 193). Radar retrievals and those from the icebreaker PWD (i.e., PWD_1) sensor show similar occurrences of snowfall (**Figure 5a** vs. **5c**), though accumulation values were quite different for particular periods (e.g., October 2019, March 2020). The ice camp PWD (i.e., PWD_2) sensor data were generally larger than those from PWD_1 (**Figure 5c** vs. **5d**). For the February through April 2020 period (and the October 31, 2019, estimate), Pluvio daily accumulations (**Figure 5b**) were significantly larger than those from other sensors.

PARSIVEL disdrometers are customarily tuned to provide the estimates of precipitation assuming rain. As a result, precipitation rates in disdrometer data files are usually not consistent with snowfall. To overcome this issue, MOSAiC PARSIVEL raw particle counts were used in this study to retrieve precipitation rates. These counts were converted to liquid-equivalent snowfall rate estimates using a snowflake particle mass–size relation $m = 0.0053D^{1.9}$ (cgs units), which was used in previous studies (e.g., Matrosov and Heymsfield, 2017). The icebreaker PARSIVEL disdrometer (i.e., $PARSIVEL_1$) was operational on most of the days during the drift, though often it did not provide data for extended periods during those days. The ice camp PARSIVEL disdrometer (i.e., $PARSIVEL_2$) was operational only intermittently and it did not provide sensible data (**Figure 5f**). The Siphon and AOS precipitation gauges did not produce sensible precipitation intensity/accumulation data throughout the entire MOSAiC deployment; thus, measurements from these gauges were not considered in this study.

3.3. Monthly accumulations

As an example, **Figure 6** depicts the time series of liquid water equivalent snowfall accumulation for November 2019 and April 2020 as estimated from different sources. There was a period between approximately 00:00 UTC on

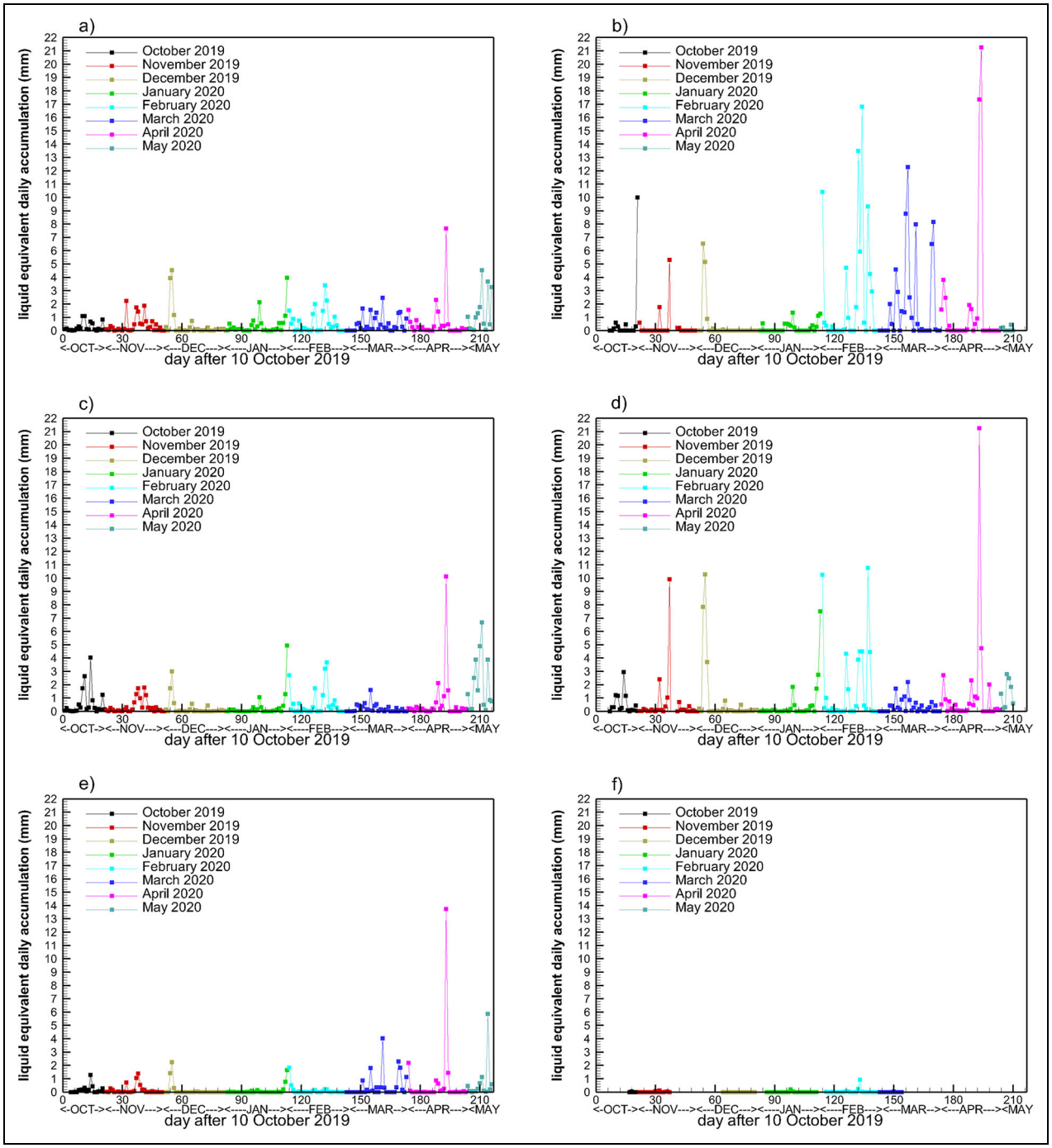

Figure 5. Daily 24-h liquid-equivalent snowfall accumulations during Multidisciplinary drifting Observatory for the Study of Arctic Climate as obtained from (a) K_a-band zenith-pointing radar measurements at 0.17 km above the ground, (b) Pluvio, (c) PWD_1, (d) PWD_2, (e) $PARSIVEL_1$, and (f) $PARSIVEL_2$ data. October 11, 2019, is Day 1. PWD = present weather detector; PARSIVEL = particle size and velocity. DOI: https://doi.org/10.1525/elementa.2021.00101.f5

November 17, 2019 and approximately 10:20 UTC on November 20, 2019, when ice camp instruments were not operational due to a power outage. Note that for the period of inactivity of the ice camp sensors during this period (**Figure 6a**), KAZR-based estimates of snowfall accumulation were approximately 3.3 mm. With this 3.3 mm addition, the Pluvio gauge November 2019 total accumulation is not that different from the radar-based estimates, though this gauge did not record any snowfall after November 20, 2019, while other sensors indicated appreciable snowfall.

As seen from **Figure 6**, the $PARSIVEL_1$ estimates of accumulation are rather close to the KAZR retrieval for April 2020 but only half of that for November 2019. $PARSIVEL_1$ accumulation data are also significantly lower compared to the results from other MOSAiC sensors for December 2019 and January 2020 (**Table 1**). It should also be mentioned that PARSIVEL data were earlier found

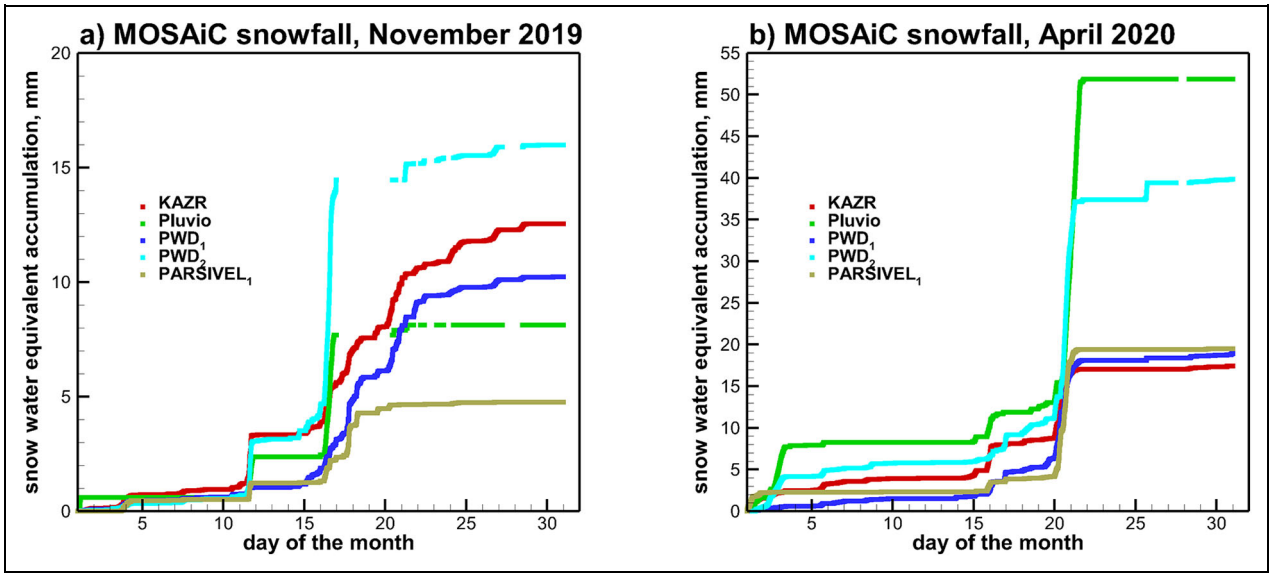

Figure 6. (a) November 2019 and (b) April 2020 liquid-equivalent snowfall accumulation from different Multidisciplinary drifting Observatory for the Study of Arctic Climate sensors. Pluvio and PWD_2 data are from the ice camp site, whereas other sensors were on the icebreaker. KAZR estimates are at the height of approximately 0.17 km above the ground and the $Z_e = 63S^{1.2}$ relation. PWD = present weather detector; KAZR = K_a-band zenith-pointing radar. DOI: https://doi.org/10.1525/elementa.2021.00101.f6

Table 1. Estimates of snow water equivalent accumulation (in mm) during different months of the MOSAiC expedition. DOI: https://doi.org/10.1525/elementa.2021.00101.t1

Sensor/Month	10/19	11/19	12/19	01/20	02/20	03/20	04/20	05/20	Total
KAZR (0.17 km)	5.9	12.5	12.1	12.3	17.1	16.3	17.4	17.9	111.5
PWD_1	12.9	10.2	7.2	9.4	16.6	6.3	18.9	27.1	108.6
PWD_2	8.3	16.0	24.1	15.9	47.1	11.4	39.9	9.5	172.2
Pluvio	11.9	8.1	12.8	7.3	72.6	60.7	54.2	0.9	228.5
$PARSIVEL_1$	3.1	4.8	4.0	2.9	3.3	13.8	19.5	9.4	60.8
KAZR (0.23 km)	6.7	14.1	14.7	13.5	19.1	18.1	19.7	20.5	126.4

Radar-based estimates are shown as derived using the $Z_e = 63S^{1.2}$ relation. Subscripts 1 and 2 for sensor abbreviations refer to the icebreaker and ice camp locations, correspondingly. The icebreaker/ice camp sensor period is October 11, 2019, to May 14, 2020/ October 17, 2019, to May 7, 2020. PWD_2 and Pluvio sensors did not operate during a period from approximately November 17, 2019, until approximately November 20, 2019. MOSAiC = Multidisciplinary drifting Observatory for the Study of Arctic Climate; PWD = present weather detector; KAZR = K_a-band zenith-pointing radar; PARSIVEL = particle size and velocity.

to have significant uncertainties for measurements of solid precipitation (Battaglia et al., 2010).

Table 1 shows monthly liquid-equivalent snowfall accumulation data as obtained from different MOSAiC ARM ground-based instruments during the period of the drift. It can be seen from **Table 1** that except for the first half of the deployment, Pluvio gauge estimates of accumulation are disparate from most other sensor results. This includes a period of very large Pluvio accumulations for the February–April 2020 period. For most of the observational period, $PARSIVEL_1$ disdrometer snowfall measurements for monthly totals were also not consistent with radar-based estimates.

As mentioned in the previous section, there was a time period during March 9 and 10, 2020 when the KAZR was not operational during precipitation. According to the PWD_1 sensor, there was about 0.3 mm of liquid-equivalent snowfall accumulation during this period. This amount was added to the KAZR-based March 2020 estimates shown in **Table 1**. Additionally, KAZR measurements in October 2019 had some artifacts mostly affecting low reflectivity data. This could result in higher than usual uncertainties in retrievals of low snowfall rates (less than about 0.02 mm h^{-1}).

As was also the case at the ARM NSA site (Section 2), in the lowest radar range gates, there was often a decreasing trend of MOSAiC KAZR-based snowfall rates with diminishing height above the ground. This decrease could be due to snowfall sublimation or/and because of some distortion of radar echo signals at shorter ranges. In addition

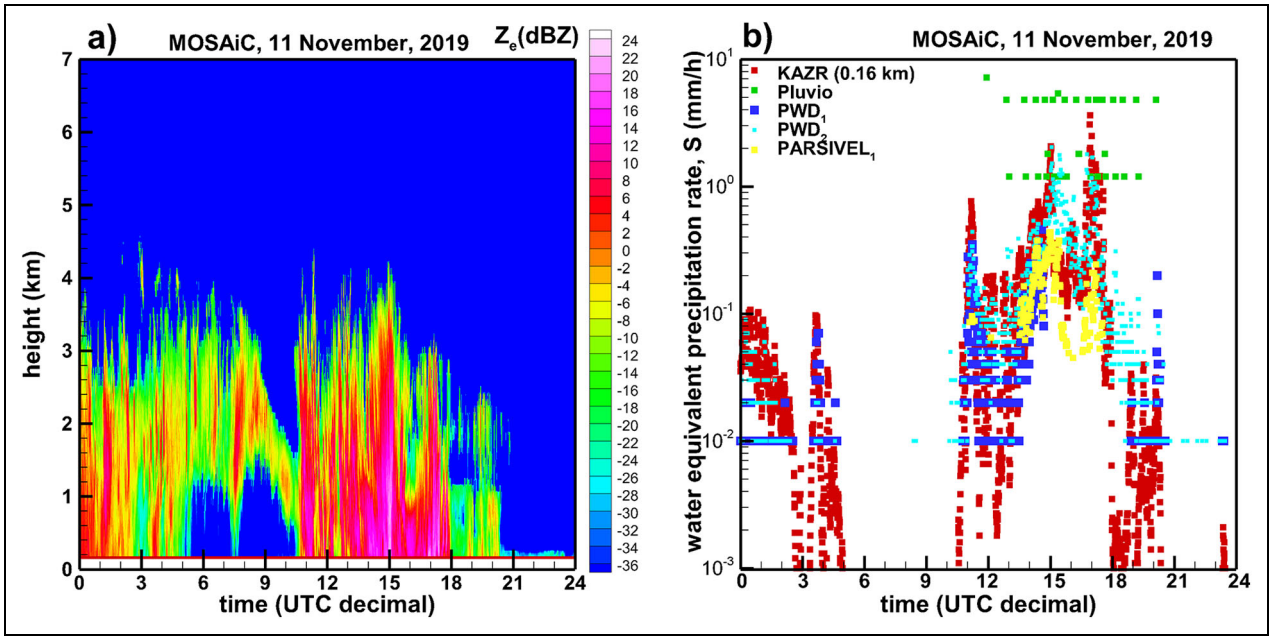

Figure 7. (a) Time-height cross sections of observed KAZR reflectivities and (b) near surface estimates of snowfall rates from different MOSAiC precipitation sensors on November 11, 2019. Pluvio and PWD_2 data are from the ice camp site, whereas other sensors were on the icebreaker. PWD = present weather detector; KAZR = K_a-band zenith-pointing radar. DOI: https://doi.org/10.1525/elementa.2021.00101.f7

to the radar-based results at 0.17 km above the ground level (AGL), **Table 1** shows KAZR-based estimates at a range gate height of 0.23-km AGL. As seen from **Table 1**, a mean decreasing trend was present for all months. If the mean vertical gradient of snowfall rate between 0.17 and 0.23 km range gate heights is assumed to be representative also for the layer below 0.17 km, where no reliable radar data exit, near surface estimates of snowfall will be smaller than those at 0.17 km by about 10%–15%. The use of the earlier relation of $Z_e = 56S^{1.2}$ (Matrosov, 2007) instead of $Z_e = 63S^{1.2}$ would result in an increase of radar-based snowfall retrievals by approximately 10% compared to those in **Table 1**.

One striking result is a general mutual inconsistency of two identical Vaisala PWD precipitation sensors, which were deployed only several hundred meters apart (i.e., onboard the icebreaker and in the adjacent sea-ice camp). As in the case with the NSA snowfall retrieval tests (Section 2), the ice camp PWD_2 precipitation sensor measured, on average, significantly larger snowfall accumulations (compared to the radar-based results) during the October 2019–February 2020 period. The PWD_1 sensor deployed onboard the icebreaker provided accumulation estimates that were, on average, similar to the radar-based retrievals for the total amounts. Although different wind conditions (and hence differences in potential blowing snow effects) at the PWD sensor locations might contribute to the discrepancy of their snowfall intensity measurements, it is problematic to attribute significantly dissimilar accumulation results only to a difference in wind effects. Analyzing instantaneous snowfall flux/rate estimates from different MOSAiC sensors provides additional insights.

3.4. Instantaneous snowfall rates

The temporal resolution of KAZR reflectivity measurements during MOSAiC was 2s. Snowfall rates derived from radar data were estimated at this resolution and then averaged in 30-s intervals. Estimates from the Pluvio, PWD, and PARSIVEL precipitation sensors were available at a 1-min resolution. Examples of precipitation rate retrievals and corresponding time-height KAZR reflectivity cross sections for several representative significant MOSAiC snowfall events are shown in **Figures 7**–**9**. These cases are meant to highlight some of the key distinctions and implications of the different observational approaches.

Maximum KAZR reflectivity values on November 11, 2019 **(Figure 7)**, were among the strongest observed during MOSAiC and, at times, they exceeded 22 dBZ. Near surface air temperature during this event varied approximately between −16 and −26°C. A general description of MOSAiC meteorological events is also given by Shupe et al. (2022). Liquid-equivalent snowfall accumulation for November 11, 2019, was around several millimeters even though there were noticeable differences among estimates from different precipitation sensors (**Figure 6a**). The bulk of snowfall accumulation was observed between approximately 11:00 and 18:00 UTC.

The Pluvio weighing gauge resolution of accumulated melted snow is 0.01 mm. Given the temporal resolution of 1 min, this corresponds to a 0.6-mm h^{-1} minimal detectable precipitation rate. However, as for the CRN gauge at the NSA ARM site (Section 2), the Pluvio gauge most often recorded several minimal increments at a time, which resulted in larger estimates of precipitation rates at the times of these incremental increases in accumulation

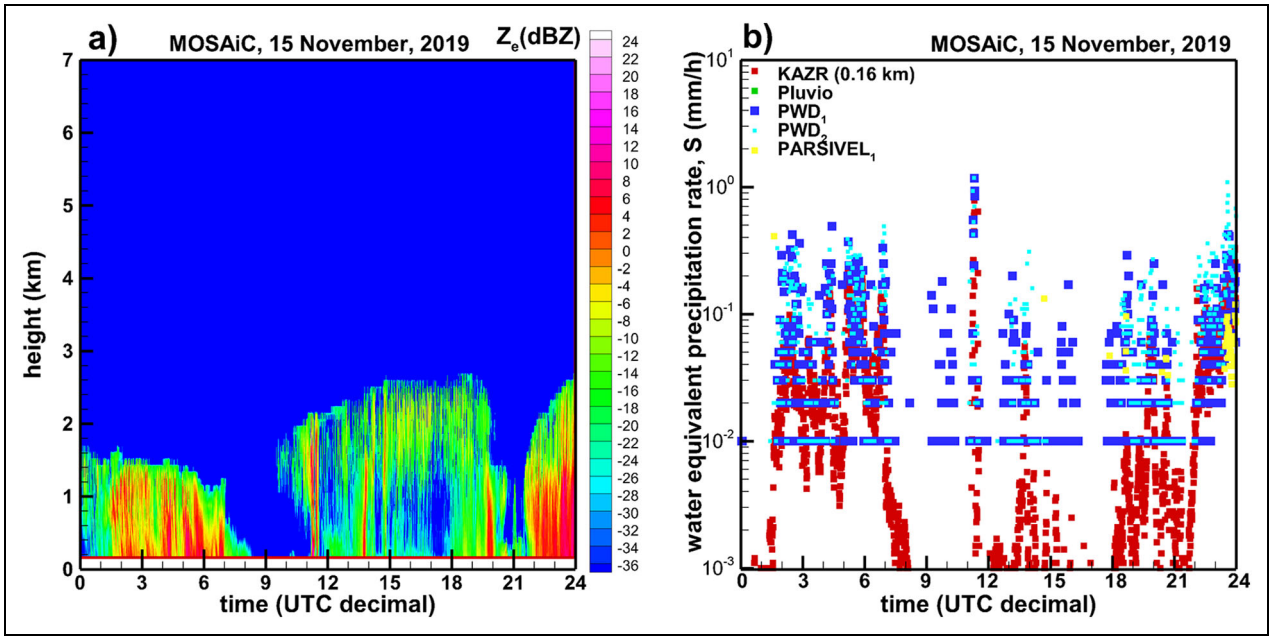

Figure 8. Same as Figure 7 but for November 15, 2019. DOI: https://doi.org/10.1525/elementa.2021.00101.f8

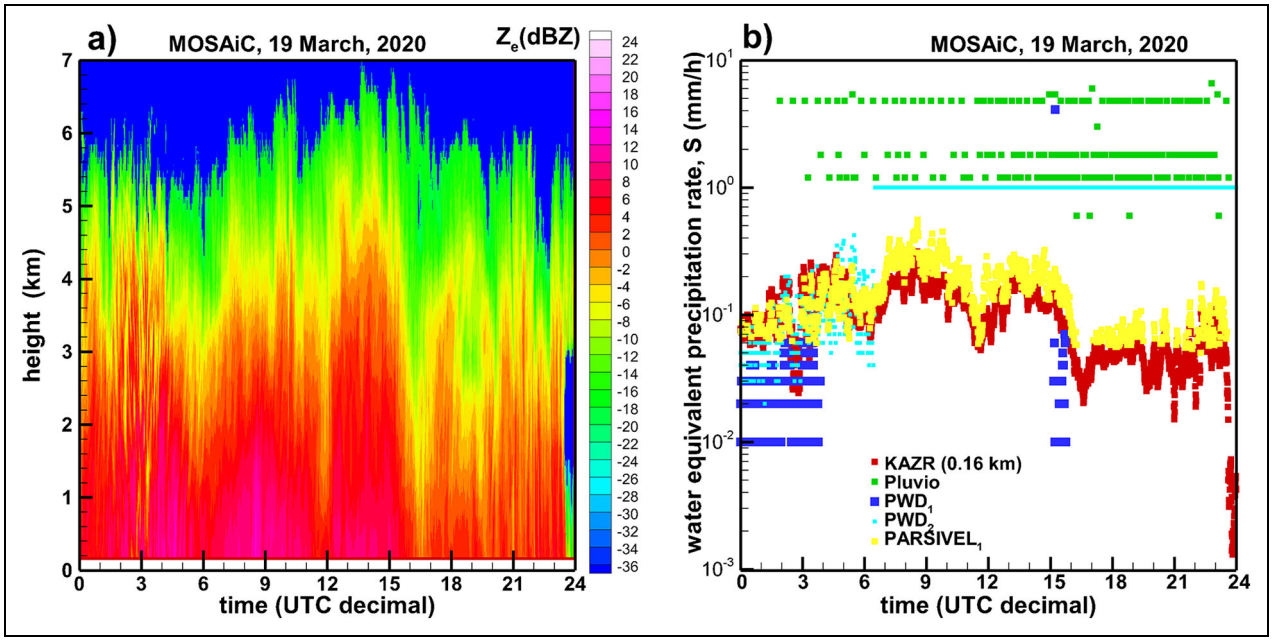

Figure 9. Same as Figure 7 but for March 19, 2020. DOI: https://doi.org/10.1525/elementa.2021.00101.f9

measurements (**Figure 7b**). These times were often separated by extended periods when Pluvio-based precipitation rates were estimated as 0 mm h^{-1} even though snowfall was continuous as seen by other precipitation sensors and radar measurements. High snowfall rate estimates from the Pluvio gauge (e.g., levels of 1.2, 1.8, . . . , 4.8 mm h^{-1} in **Figures 7b** and **9b**) correspond to the increases of its accumulated melted snow measurements, which are multiples of the minimal increment of 0.01 mm (e.g., 0.02, 0.03, . . . , 0.08 mm). These high 1-min resolution snowfall rate estimates, however, are separated by the values of 0 mm h^{-1} for the times when there were no incremental increases in accumulation.

Additionally, the Pluvio gauge did not indicate accumulations outside the period between 11:00 and 18:00 UTC on November 11, 2019 (**Figure 7b**), and did not record any precipitation on November 15, 2019 (**Figures 5b** and **8b**), even though some significant snowfall was observed by other sensors. Later in the deployment, Pluvio significantly overestimated snowfall compared to other precipitation sensor data (**Table 1** and **Figures 5b** and **9b**).

The precipitation rate resolution of PWD optical sensors is 0.01 mm h^{-1}. During some periods, there was an approximate agreement between snowfall rate estimates from both PWD sensors (e.g., a snow shower at around

11:00 UTC on November 11, 2019; **Figure 7**). However, very often (e.g., **Figure 9b**), these sensor measurements were noticeably different. The optical sensor onboard the icebreaker (PWD_1) reported an error in precipitation rate estimates (even though it was otherwise operational) during the period of most significant snowfall between approximately 14:40 and 18:30 UTC on November 11, 2019 (**Figure 7b**), and for most of the event on March 19, 2020 (**Figure 9b**). During the March 19, 2020, event, which was characterized by relatively low near surface wind (<5 m s^{-1}), the ice camp optical sensor (PWD_2) continuously recorded precipitation rate of exactly 1 mm h^{-1} from about 6:30 UTC, which likely was an artifact. As mentioned above, such obvious artifact data were excluded when calculating daily and monthly accumulations.

According to the AOS surface meteorology observations, wind speed during an event of November 11, 2019, was generally between 10 and 15 m s^{-1} (not shown). Given such conditions, some blowing snow affecting measurements of surface-based sensors could be expected. No significant erroneous snowfall rate measurements were, however, recorded during the period between about 05:30 and 09:40 UTC (except a few PWD_2 measurements of 0.01 mm h^{-1}) when according to the radar data (**Figure 7a**), there was no echo in the vertical atmospheric column above the lowest radar range gate and hence no precipitation. On the other hand, there was some evidence of possible blowing snow effects between approximately 20:30 and 23:30 UTC (**Figure 7b**) with a significant number of PWD_2 estimates of 0.01 mm h^{-1} during this time interval. For rather short time intervals, possible blowing snow contributions in the radar data are seen at approximately 23:00 UTC (**Figure 7b**). The corresponding estimates of snowfall rates, however, are less than about 0.002 mm h^{-1}, which does not significantly affect corresponding total accumulations.

The snowfall shown in **Figure 8** corresponds to a warm front passage of a cyclone at about 10:00 UTC on November 15, 2019. As a result of the frontal passage, the temperature increased to approximately −5°C (not shown). Precipitation was observed throughout the day, except for a period between about 08:20 and 11:00 UTC, when the radar did not observe any significant echo (**Figure 8a**). All ARM precipitation sensors except the icebreaker-based PWD_1 optical gauge did not detect any precipitation signal during this time. Nonzero PWD_1 estimates of precipitation rates during this period were between about 0.01 and 0.2 mm h^{-1} (**Figure 8b**), even though such estimates were not continuous and they likely represented spurious data.

The icebreaker $PARSIVEL_1$ disdrometer measurements did not indicate any precipitating particles during extended periods of observations such as those before about 11:00 UTC and after 18:00 UTC on November 11, 2019 (**Figure 7b**), and for most of the events on November 15, 2019 (**Figure 8b**). As a result, disdrometer-based monthly snowfall accumulations were often lower than most other sensor estimates (**Table 1**). Surprisingly, when disdrometer particle counts were available, the corresponding PARSIVEL-based precipitation rates were often rather consistent with radar-based retrievals (e.g., **Figure 9b**) even though there is appreciable data scatter.

Although data from only 3 MOSAiC days are shown here (**Figures 7**–**9**), the issues highlighted concerning snowfall rate estimates from different sensors are common for the entire MOSAiC snowfall data set and for snowfall measurements more broadly (e.g., Rasmussen et al., 2012). Even though total accumulation amounts for the whole October 2019–May 2020 icebreaker drifting period from different sensors could be similar, these are often the results of different instantaneous, daily, and monthly snowfall data (e.g., PWD_1 results vs. KAZR-based estimates).

Figure 10 shows the scatter plots of 0.01 of the Julian day snowfall rate averages (i.e., approximately 15-min averages) as inferred from different sensors during the October 17, 2019, to May 6, 2020, period when all precipitation sensors were deployed. This time averaging was chosen, in part, due to the fact that comparisons involved measurements taken at 2 different locations and with a variety of different sample resolutions. The scatter plots represent times when both sensors in a given scatter plot recorded snowfall (i.e., $S > 0$ mmh^{-1}). Radar data represent retrievals for the approximately 0.17 km height above the ground. The corresponding statistical metrics of NB and NMAD of a *Y*-axis variable as compared to the *X*-axis variable are also given in **Figure 10**.

As seen in **Figure 10**, there is a satisfactory mean correspondence between the radar estimates and those from $PARSIVEL_1$ for the time periods when the disdrometer was reporting particle counts. It should be mentioned, however, that disdrometer snowfall rate estimates are rather strongly dependent on the assumption of snowflake mass–size relation. Note also that $PARSIVEL_1$ existing data points with $S < 0.1$ mm h^{-1} are significantly less numerous compared to the other sensors in **Figure 10**. As expected from comparing monthly accumulations, PWD_2 measurements significantly overestimate snowfall rates compared to the radar-based retrieval and also to PWD_1 measurements. Mean PWD_2 snowfall rate measurements exhibit the lowest correlation with results from other sensors.

While **Figure 10** shows the different data correspondences when both snowfall rate estimates for a given pair of sensors exist, some amount of precipitation was measured by a particular sensor when no KAZR echoes were present. Judging from approximately 15-min snowfall rate averages, for PWD_1 and PWD_2 sensors, these amounts were about 5 and 18 mm of liquid-equivalent accumulation, respectively. At least in part, these accumulations might be attributed to blowing snow effects. Conversely, KAZR-based accumulations were around 14 mm (19 mm) when PWD_1 (PWD_2) did not record any precipitation and was not operational or provided obvious artifacts. Practically, no $PARSIVEL_1$-based accumulations were recorded for the period of no KAZR echo. About 40 mm of accumulation was retrieved from KAZR data when there was no information on icebreaker $PARSIVEL_1$ particle counts

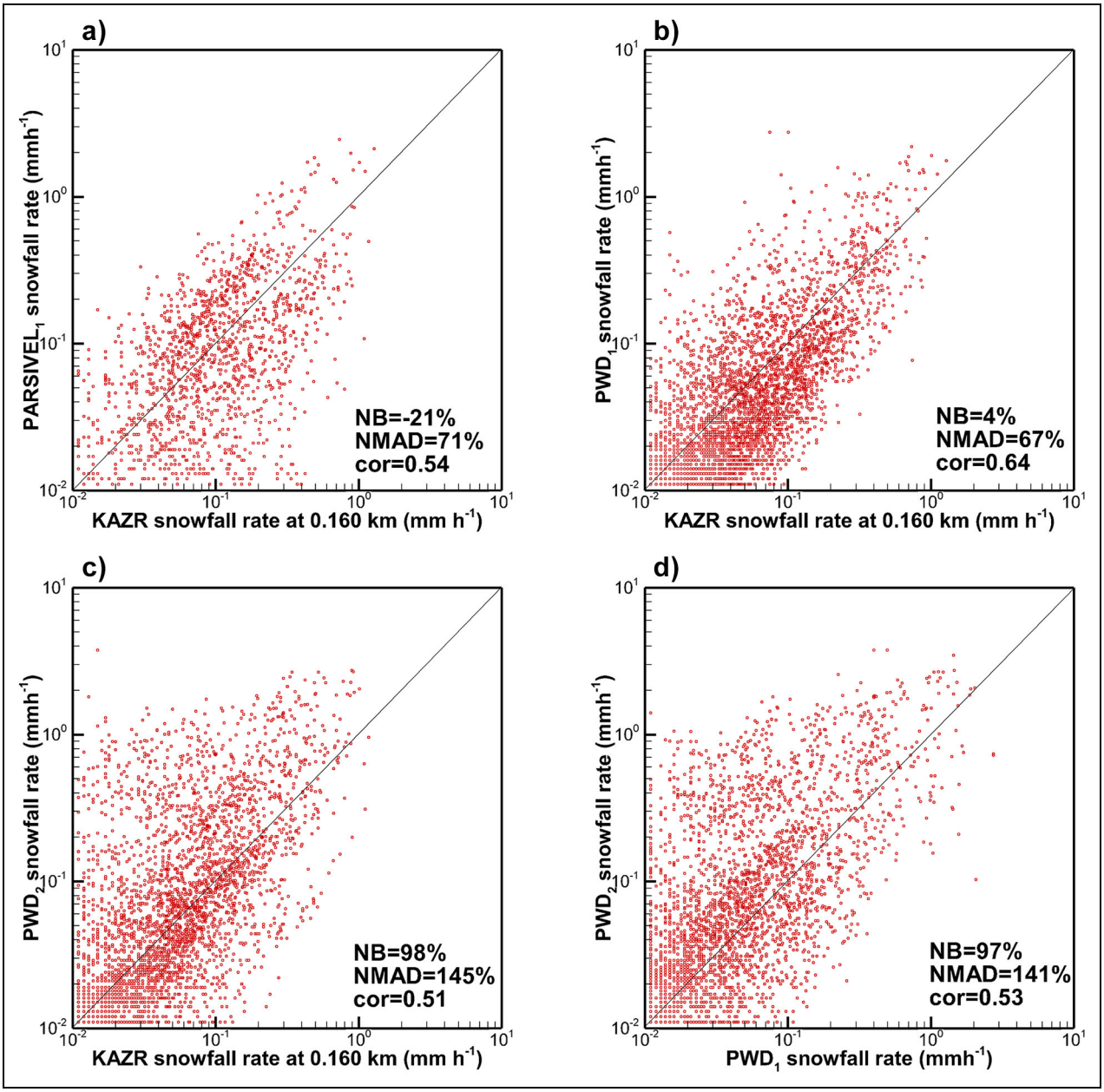

Figure 10. Scatter plots of 0.01 Julian day averages of snowfall rates: (a) KAZR-based estimates versus PARSIVEL$_1$ estimates, (b) KAZR estimates versus PWD$_1$ estimates, (c) KAZR-based estimates versus PWD$_2$ estimates, and (d) PWD$_1$ estimates versus PWD$_2$ estimates. The data are for time periods when both estimates are greater than 0. PWD = present weather detector; KAZR = K_a-band zenith-pointing radar; PARSIVEL = particle size and velocity. DOI: https://doi.org/10.1525/elementa.2021.00101.f10

even though this disdrometer was nominally operational most of the time.

To evaluate some possible effects of wind conditions on snowfall estimates, **Figure 11** depicts the differences in snowfall rates from different sensors versus mean near surface wind speeds. The data samples of snowfall rates from **Figure 10** were used also in **Figure 11**. There are no obvious trends in the differences between KAZR-based retrievals and PARSIVEL$_1$ or PWD$_1$ estimates as a function of wind speed (**Figure 11a** and **b**). There is, however, an indication that PWD$_2$ snowfall rate estimates become noticeably higher, on average, compared to estimates from other sensors for wind speed greater than about 13–14 m s^{-1} (**Figure 11c** and **d**). Part of this increase in PWD$_2$ estimates might be due to a contribution of blowing snow as previously discussed for the November 11, 2019, event (**Figure 7**).

As can be seen from **Figure 10**, overall snowfall rates during MOSAiC were mostly smaller than 1 mm h^{-1} and the frequency of occurrence of smaller snowfall rates was higher. It is instructive to estimate quantitively what are typical snowfall rates that contribute most to the total accumulation. Based on radar retrievals, **Figure 12** shows relative contributions of snowfall of different intensities to the total accumulation. About half of the total accumulation can be attributed to snowfall with liquid-equivalent precipitation rates less than approximately 0.2 mm h^{-1}. Heavier snowfall with precipitation rates greater than 2 mm h^{-1} comprised

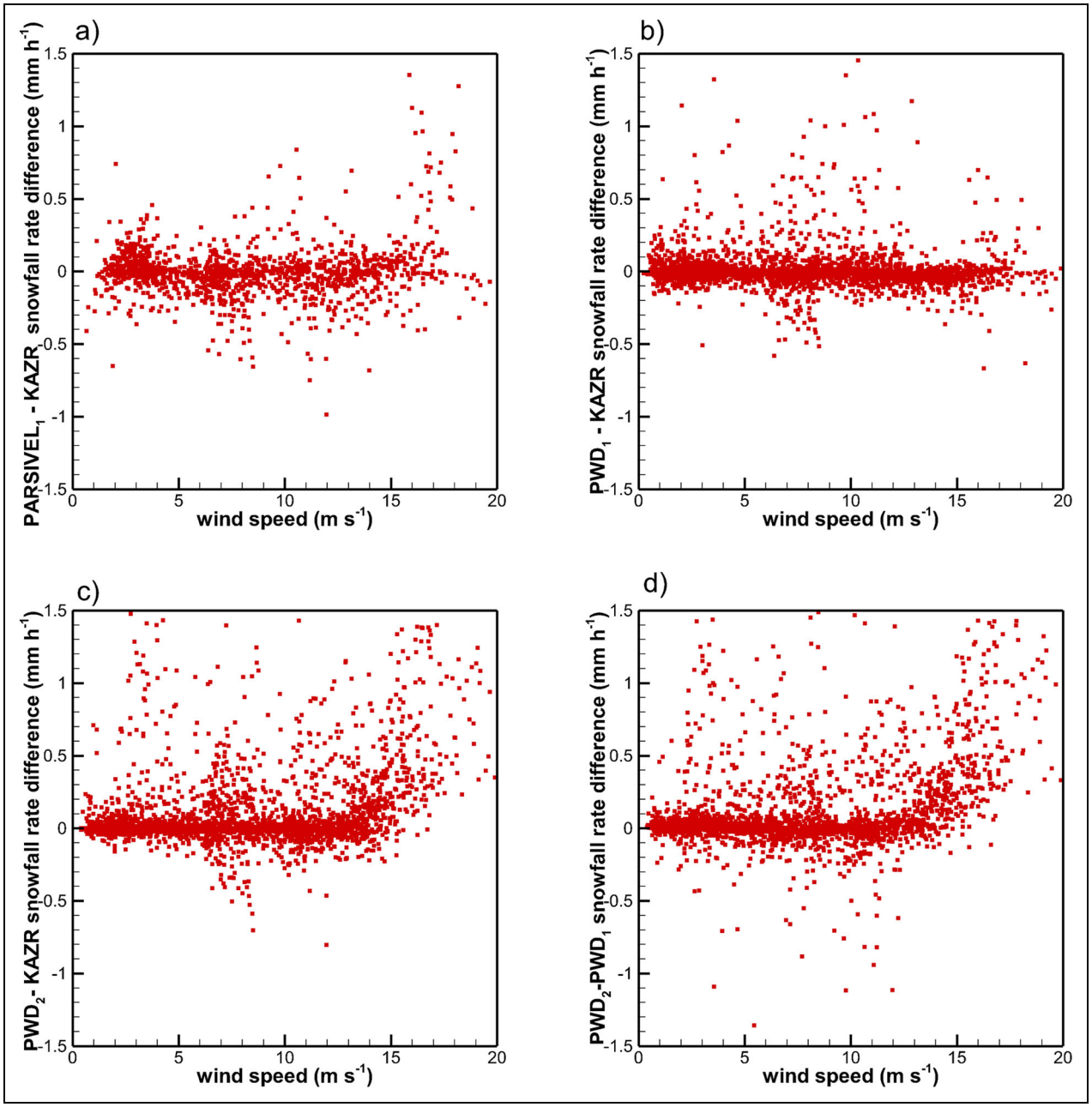

Figure 11. Scatter plots of 0.01 Julian day (approximately 15 min) average snowfall rates from different MOSAiC sensors versus wind speed: (a) $PARSIVEL_1$–KAZR estimate differences, (b) PWD_1–KAZR estimate differences, (c) PWD_2–KAZR estimate differences, and (d) PWD_2–PWD_1 estimate differences. MOSAiC = Multidisciplinary drifting Observatory for the Study of Arctic Climate; PWD = present weather detector; KAZR = K_a-band zenith-pointing radar; PARSIVEL = particle size and velocity. DOI: https://doi.org/10.1525/elementa.2021.00101.f11

less than about 3% of the total accumulation. Estimates of relative contributions of snowfall of different intensities depend on a particular Z_e–S relation used and they also are sensitive to the radar absolute calibration.

Overall, the MOSAiC KAZR-based snowfall rate estimates are the most complete in terms of measurement data availability. These estimates, however (as other sensor data), are subject to uncertainties. Understanding these uncertainties could lead to more appropriate utilization of the radar-derived precipitation retrievals for different applications of MOSAiC data.

4. Uncertainties of radar-based snowfall estimates

Uncertainties in assumptions about snowflake microphysical properties and in the electromagnetic scattering model contribute to errors in radar-based snowfall retrievals through variability of Z_e–S relations. Souverijns et al. (2017) found an approximately 40% uncertainty in snowfall estimates due to variability of the relations at a K-band radar frequency (approximately 24 GHz). Additionally, possible radar calibration biases are an important factor affecting accuracy of snowfall retrievals. To demonstrate

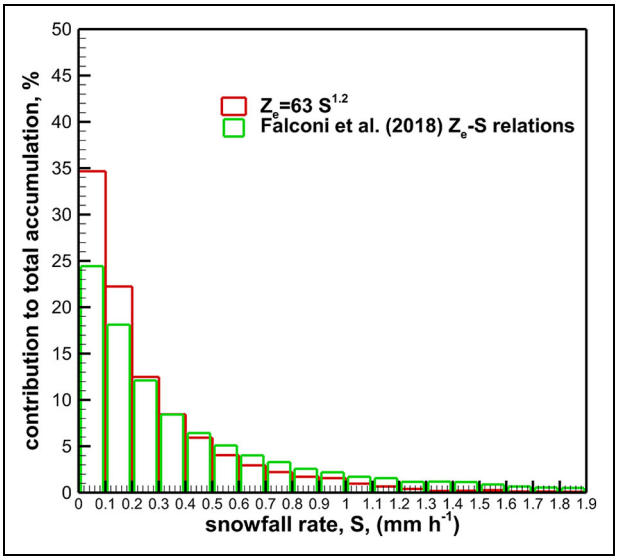

Figure 12. Relative contributions of snowfall of different rates to the total accumulation for the period from October 11, 2019, to May 14, 2020, according to the radar-based retrievals. DOI: https://doi.org/10.1525/elementa.2021.00101.f12

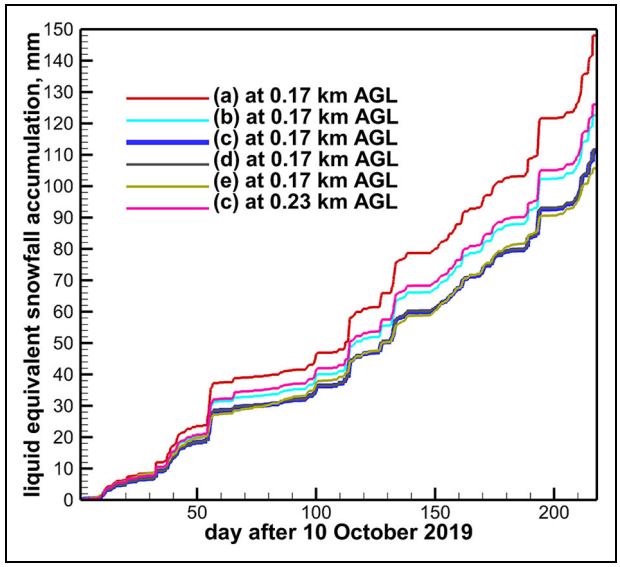

Figure 13. KAZR-based liquid-equivalent snowfall accumulations at approximately 0.17 km above the ground as estimated from different Z_e–S relations shown in Figure 1: (a) Falconi et al. (2018; their relations applied depending on liquid water path values), (b) Matrosov (2007), (c) $Z_e = 63\ S^{1.2}$ (this study), (d) $Z_e = 60.17\ S^{1.18}$, Huang et al. (2019), (e) $Z_e = 313\ S^{1.85}$, Kulie and Bennartz (2009). KAZR = K_a-band zenith-pointing radar. DOI: https://doi.org/10.1525/elementa.2021.00101.f13

uncertainties of radar-based snowfall estimates due to varying Z_e–S relations, **Figure 13** shows KAZR-based total accumulation estimates for MOSAiC obtained using the different K_a-band Z_e–S relations shown in **Figure 1**.

Since Falconi et al. (2018) provide their relations based on snowfall rime conditions, the corresponding retrieval (i.e., curve *a* in **Figure 13**) was estimated using their 3 different relations for different snow rimes in conjunction with supercooled liquid water path (LWP) in the vertical atmospheric column. According to these authors, the 3 LWP intervals corresponding to low, medium, and high rime conditions are characterized by (1) LWP < 140 gm^{-2}, (2) 140 gm^{-2} ≤ LWP ≤ 440 gm^{-2}, and (3) LWP > 440 gm^{-2}, correspondingly (their figure 3). LWP values for choosing an appropriate riming interval were obtained from the MOSAiC ARM microwave radiometer retrievals (Gaustad et al., 2019). When applying a rime-dependent Z_e–S relation from Falconi et al. (2018), LWP values were averaged in 12-min time intervals prior to the time of the radar profile. This approximately accounts for snowflake fall time in a region of supercooled liquid before reaching lower radar range gates where snowfall rate is retrieved.

In addition to snowfall accumulations obtained from different relations applied to the measurements at an altitude of approximately 0.17 km above the ground, **Figure 13** shows accumulation estimates when applied to the measurements at an altitude of 0.23-km AGL. An interesting result is that in spite of having a very different prefactor and exponent (as compared to other Z_e–S relations), relation (e) (**Figures 1** and **13**) provides results approximately similar to many other relations (**Figure 13**). This result can be explained by the fact that the largest contribution to accumulation comes from snowfall rates around 0.1–0.2 mm h^{-1} (**Figure 12**), where many different Z_e–S relations (except the relation [f]) cluster (**Figure 1**). As seen from **Figure 13**, there is an about 30% spread in accumulation estimates due to a Z_e–S relation choice. Note that relation (f) was excluded since it provides unrealistically very high snowfall estimates (approximately 700 mm of total accumulation), and its results are not shown in **Figure 13**.

Potential biases in the absolute radar calibration of reflectivity measurements are an independent source of retrieval errors. The errors associated with calibration biases could be substantial. One or 2 decibel reflectivity biases, which are not uncommon for cloud radars (Maahn et al., 2019), would result in about 20% and 40% snowfall rate retrieval errors for the Z_e–S relation exponent of 1.2. Dependencies of radar reflectivities on liquid water cloud–drizzle microphysical processes provide opportunities to assess the absolute calibration of vertically pointing radars (Maahn et al., 2019).

Although there were no liquid water cloud observations during the MOSAiC October 2019–May 2020 drift period, there were warm stratus clouds observed by the MOSAiC sensors in summer 2020. Maahn et al. (2019) suggest a reference relation between LWP and the maximum reflectivity, max(Z_e), in a vertical profile for liquid water stratus clouds (their table 4). **Figure 14a** shows a time-height cross section from a lightly drizzling warm stratus cloud observed by the MOSAiC KAZR in the GE measurement mode. **Figure 14b** depicts a scatterplot between LWP retrieved from microwave radiometer measurements and max(Z_e). As seen from **Figure 14b**, for reflectivities less than about −17 dBZ, a correspondence

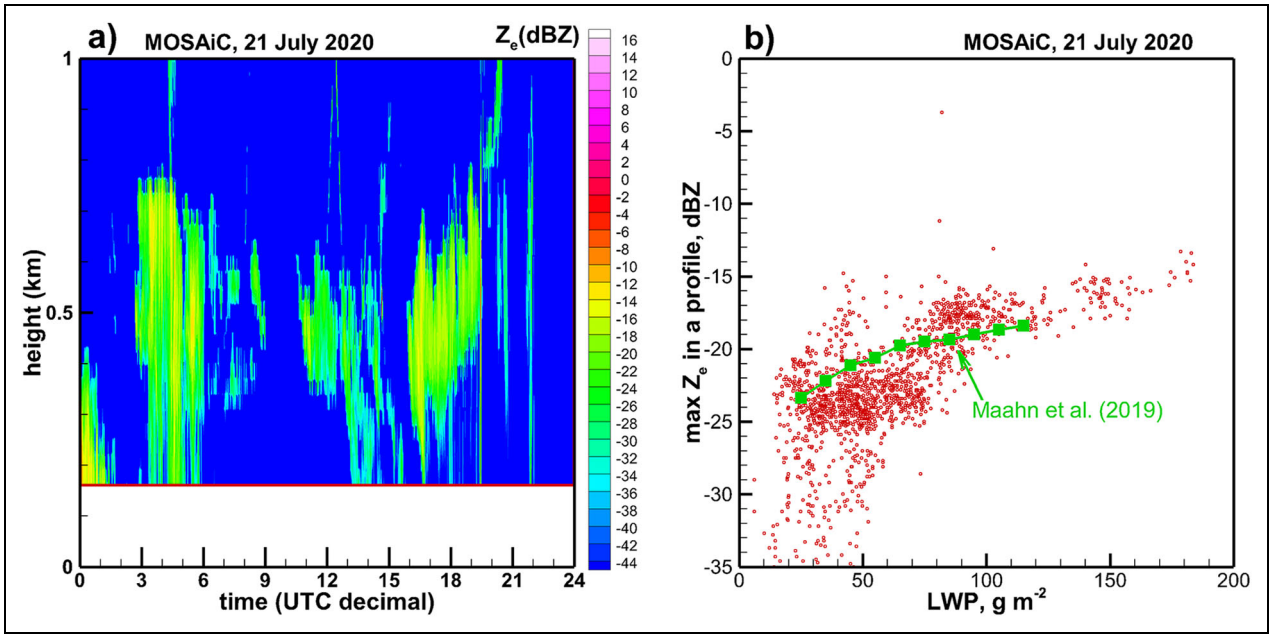

Figure 14. (a) Time-height cross section of KAZR general reflectivity for a stratus liquid water cloud observed on July 21, 2020, and (b) maximum KAZR reflectivity in a vertical profile versus liquid water path. KAZR = K_a-band zenith-pointing radar. DOI: https://doi.org/10.1525/elementa.2021.00101.f14

between LWP and max(Z_e) approximately follows that from Maahn et al. (2019) even though some substantial data scatter is present. Backscatter contributions from drizzle drops in volumes where cloud and drizzle drops coexist gradually become dominant when reflectivities are greater than approximately −17 dBZ (Maahn et al., 2019). These LWP– max(Z_e) correspondence comparisons indicate that the GE-mode MOSAiC and NSA KAZR absolute calibrations were similar.

Another way to evaluate the absolute calibration of a vertically pointing radar is to analyze long-term mean values of observed cloud reflectivities and compare them with mean values from measurements of another radar, which is believed to be well calibrated. This approach was used by Kollias et al. (2019), when they compared measurements from different vertically pointing ARM radars with *CloudSat* radar measurements. *CloudSat*, however, does not pass over the Central Arctic, so comparisons between MOSAiC KAZR and CloudSat reflectivities are not possible. Comparisons, however, can be performed between the MOSAiC and NSA radars.

Figure 15 shows mean GE-mode reflectivities observed by the MOSAiC KAZR at an altitude of 4 km as a function of the reflectivity threshold (i.e., the minimum reflectivity considered when calculating mean values). Note that the influence of sensitivity differences between the 2 radars is minimized at higher reflectivity thresholds. Also shown in **Figure 15** are corresponding values for the NSA GE-mode KAZR data, for the period of the retrievals depicted in **Figure 2**. Although there could be differences in snowfall microphysical processes (e.g., aggregation, riming) influencing reflectivities at different sites, these processes are typically active at lower altitudes, and it can be expected/assumed that at relatively high altitudes, the Arctic cloud environment is relatively similar during the cold season.

As seen from **Figure 15**, mean high-altitude reflectivity values from the NSA and MOSAiC KAZRs are rather similar. Since, as mentioned previously, the NSA KAZR was found to be relatively well calibrated (Maahn et al., 2019), the data in **Figure 15** provide some confidence in the absolute calibration of the GE mode MOSAiC KAZR. Comparing NSA and KAZR mean reflectivities at different altitudes (e.g., 5 km—not shown) provides results similar to those in **Figure 15**, although the number of observations decreases with increasing altitude.

Overall, comparisons of high-altitude mean reflectivities of ice clouds and mean correspondences between reflectivities and LWP of warm stratus clouds suggest that the absolute calibration of the GE-mode MOSAiC KAZR measurements during the MOSAiC expedition was comparable to that of the NSA KAZR. Several decibel uncertainties, however, cannot be ruled out.

Given a relatively high level of KAZR snowfall retrieval uncertainties, comparisons with measurements from various sensors/methods are important for better understanding the reliability of radar-based data. Manual measurements of snow water equivalent (SWE) on sea ice are another source of independent data, which can be used for assessing radar-based retrievals of snowfall accumulations.

SWE measurements of snow over sea ice at MOSAiC were conducted approximately weekly starting on October 31, 2019 (Wagner et al., 2021). To mitigate effects of drifting snow, these measurements were conducted along 2 transect paths and then averaged. Wagner et al. (2021) report a monotonic increase in SWE values with time until February 20, 2020, after which the SWE decreases over prolonged time periods were observed, suggesting that the snow loss was greater than its increase by falling snow. These authors explained these decreases by snow erosion

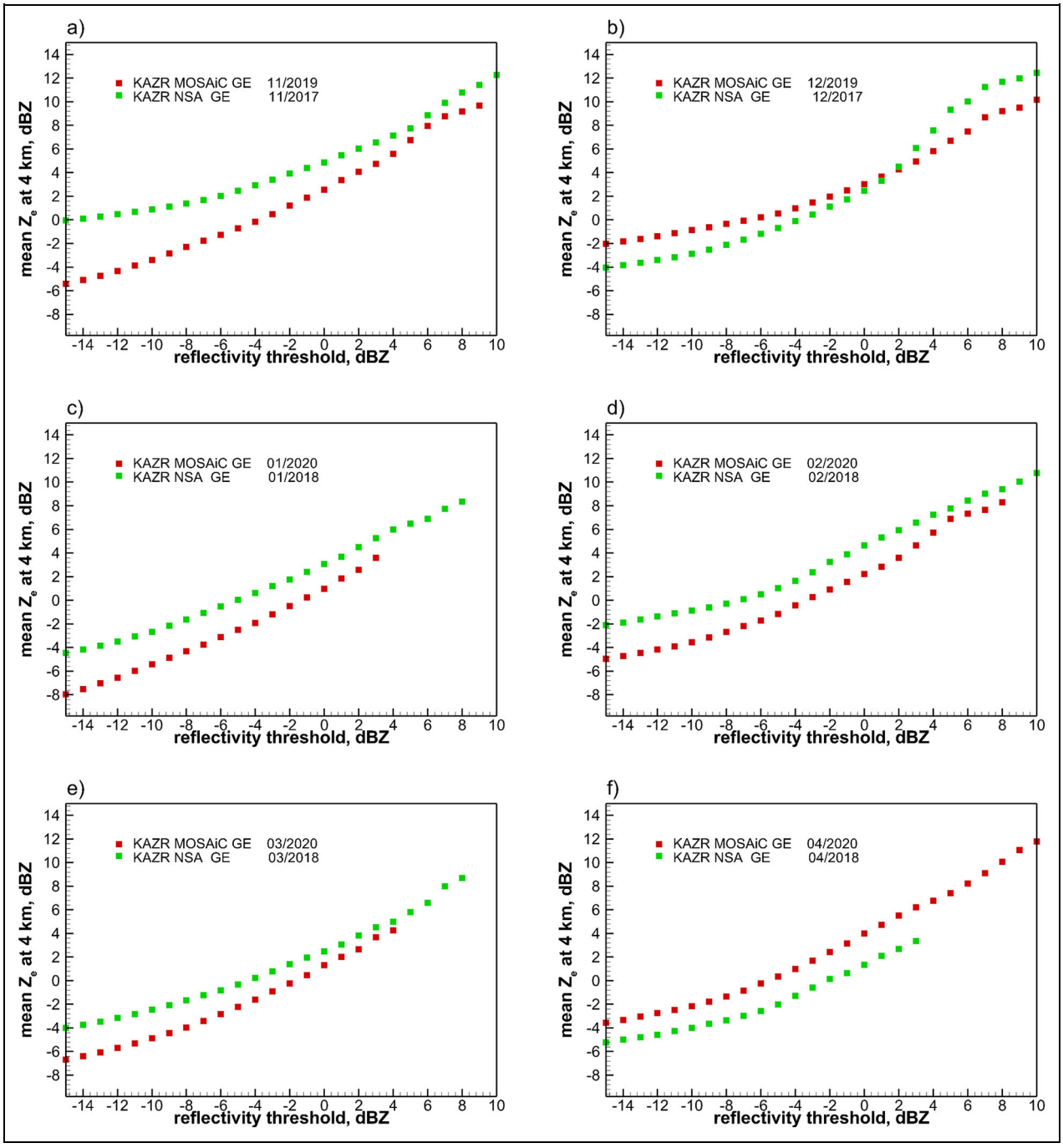

Figure 15. Mean reflectivities at a 4 km height for the MOSAiC and NSA KAZR for (a) November (b) December, (c) January, (d) February, (e) March, and (f) April. MOSAiC = Multidisciplinary drifting Observatory for the Study of Arctic Climate; KAZR = K_a-band zenith-pointing radar; NSA = North Slope of Alaska. DOI: https://doi.org/10.1525/elementa.2021.00101.f15

and suggested that no significant loss of snow occurred prior to February 20, 2020, such that SWE increase prior to this date was approximately equal to snowfall.

The total SWE increase from October 31, 2019, to 12 UTC on February 20, 2020 (i.e., the midtime of the transect SWE measurements on this day), was approximately 36 mm, although some significant uncertainties could be expected (Wagner et al., 2021, their figure 11b). The results of the KAZR-based retrievals using different Z_e–S relations for this period are shown in **Table 2**. It can be seen from this table that the radar-based retrievals generally indicate higher accumulations compared to the on-ice SWE estimates. Note also that if there were unaccounted for losses of snow on ice prior to February 20, 2020 (e.g., losses due to sublimation and/or erosion processes undetected against the background of a general SWE increase due to snowfall), the corresponding SWE of fallen snow on ice could be higher than the estimate of 36 mm. **Table 2** also shows the snowfall accumulation from the fifth-generation European Centre for Medium-Range Weather Forecasts Atmospheric Reanalysis (ERA5) as reported by Wagner et al. (2021, their figure 11b). While

Table 2. Radar-based snowfall accumulations for the period 00:00 UTC November 1, 2019, to 12:00 UTC February 20, 2020, from different Z_e–S relations and the corresponding SWE of snow on ice estimate. DOI: https://doi.org/10.1525/elementa.2021.00101.t2

***Ze*–*S* Relation/SWE**	**(a)**	**(b)**	**(c)**	**(d)**	**(e)**	**(c)**	**SWE**	**ERA5**
Height AGL, km	0.17	0.17	0.17	0.17	0.17	0.23	0.0	0.0
Accumulation, mm	67.7	56.6	51.3	51.6	48.6	58.4	~36.	~56.

Relation notations as in **Figure 13**. Height above the ground level (AGL) accounts for the height of radar location on the icebreaker.

the ERA5 estimates and radar-based retrievals are remarkably similar, there are likely significant uncertainties in each of these data sets. A comprehensive analysis of the ERA5 snowfall is needed but is beyond the scope of this study.

5. Discussion and conclusions

Vertically pointing GE-mode measurements from the ARM KAZR radar were used to retrieve high temporal resolution (30 s) snowfall rates/fluxes during the first drift of the MOSAiC expedition. The radar measurements were available during practically the entire time of the MOSAiC icebreaker drift from October 11, 2019, to May 14, 2020 (with an exception of 18:00 UTC March 9 to 14:00 UTC March 10, 2020). According to the radar-based retrievals, total liquid-equivalent snowfall accumulation was around 110 mm (**Table 1**). Accumulations from other MOSAiC ground-based and ship-based sensors for the same period varied from approximately 60 to 230 mm. About half of the total MOSAiC liquid-equivalent accumulations came from snowfall with precipitation rates less than about 0.2 mm h^{-1}.

The radar-derived snowfall rates were retrieved at heights 0.17- to 0.25-km AGL. At these heights, the effects of blowing snow, which could be substantial near the ground (Rasmussen et al., 2012), are expected to be negligible. While radar echoes from blowing snow might infrequently reach these heights for short periods of time, corresponding retrieved snowfall rates during these periods are typically less than about 0.002 mm h^{-1}, and their contribution to radar-derived accumulations is negligible.

For the time when both radar-based and Vaisala optical sensor data were available, the icebreaker-based PWD_1 and KAZR-derived mean snowfall rates showed little mutual bias (approximately 9%), though there were time periods when only radar or only PWD_1 sensor data existed. The ice camp-based PWD_2 sensor snowfall rates were biased high (with a normalized relative bias of around 100%) relative to both KAZR-derived and PWD_1 data. At higher wind speed, there were indications of blowing snow effects to this on-ice Vaisala optical sensor, which is consistent with the results of comparisons using a similar instrument at the ARM NSA facility. A relatively good agreement between PWD_1 and KAZR-derived total accumulations is, in part, due to mutual compensations among the periods, when PWD_1 was not providing measurements during significant snowfall events, and periods, when this sensor indicated measurable snowfall whereas other sensors indicated no precipitation and the KAZR did not detect any radar echo in the vertical atmospheric column. The reasons for discrepancy between 2 identical sensors (PWD_1 and PWD_2) are not totally understood, though differences in the sensor deployment locations (approximately 2-m AGL in the ice camp and approximately 22-m AGL onboard the icebreaker) and associated differences in wind conditions could be a factor.

The Pluvio gauge measurements, while being suitable for accumulation measurements, did not provide high time resolution snowfall rate estimates. Like other weighing precipitation gauges (e.g., the CRN Geonor DFIR gauge in Utqiaġvik, AK), the Pluvio gauge measures only incremental accumulation. Although the incremental accumulation resolution of 0.01 mm allows for estimating Pluvio precipitation rate in increments of 0.6 mm h^{-1}, typically several 0.01-mm minimal increments occurred for each change in Pluvio accumulation. This resulted in the fact that Pluvio gauge snowfall rate estimates were only sparsely available, and the corresponding values were much larger than estimates from the other MOSAiC instruments. During the second part of the drift (February–April 2020), this gauge's monthly accumulations were significantly higher than those for all other MOSAiC sensors.

The $PARSIVEL_1$ disdrometer on the icebreaker did not provide snowflake particle measurements during extended periods when other sensors indicated precipitation. Typically, this disdrometer's measurements are tuned for measuring rain drops. In this study, information on raw particle counts was used to infer snowfall rates from disdrometer data. During periods when particle size distributions were available, disdrometer-based snowfall rate estimates generally corresponded to the trends in radar-based retrievals though some appreciable data scatter existed. PARSIVEL estimates, however, are strongly dependent on the assumption about snowflake mass-size relations used to calculate snowfall rates. Due to this dependence and also because of unavailability of disdrometer data during many periods of MOSAiC snowfall, the use of PARSIVEL data for inferring snowfall rates is rather limited to specific cases.

The use of different K_a-band reflectivity–snowfall rate relations applied to KAZR measurements results in uncertainty of radar-based retrievals. Applying several relations suggested recently in various studies resulted in a spread

of at least 30% in estimated total snowfall accumulation for a given range gate height. For the MOSAiC period, all Z_e–S relations considered here provided total accumulation results that were greater than manual snow estimates made on the ice. While the manual on-ice measurements might be biased low as a result of underestimating snow erosion from the surface, it is also possible that the MOSAiC KAZR reflectivities had an absolute calibration bias. Possible MOSAiC KAZR absolute calibration biases will result in biases in snowfall retrievals. For the Z_e–S relation used here, a reflectivity bias of ΔZ (in decibels) would bias snowfall rate retrievals by a factor of $[10^{(\Delta Z/10)}]^{(1/1.2)}$ (e.g., 21% increase/18% decrease for a 1 dB increase/decrease in reflectivity, or 47% increase/32% decrease for a 2 dB increase/decrease in reflectivity). Assuming the independence of errors due to the variability in the Z_e–S relations and those in the absolute radar calibration, snowfall rate retrieval uncertainties of around 50% can be expected (for an approximately 2-dB calibration error). Additionally, there is uncertainty in how the radar-based snowfall rates derived at approximately 0.17-km AGL are related to those at the surface.

Overall, KAZR-based retrievals were the most consistent source of instantaneous snowfall rate estimates during MOSAiC in terms of the data availability. Compared to other sensors, they are expected to be the least affected by artifacts due to blowing snow. While retrieval uncertainties could be significant, these radar-based estimates are an important addition to the other available perspectives on MOSAiC snowfall and can be useful for a wide range of studies examining atmospheric processes and atmosphere–surface coupling. The high temporal resolution radar-based MOSAiC snowfall rate/flux data based on retrievals using the $Z_e = 63\ S^{1.2}$ relation is provided to the ARM archive (Matrosov et al., 2022; https://doi.org/10.5439/1853942).

Data accessibility statement

All the measurement data used in this study are publicly available online from the ARM user facility archive: https://www.archive.arm.gov/data/. Data streams for individual instruments from the ARM archive are also listed in the reference list.

Acknowledgments

The National Oceanic and Atmospheric Administration Physical Sciences Laboratory's resources were used when conducting this study. Data were obtained from the Atmospheric Radiation Measurement Program sponsored by the U.S. Department of Energy, Office of Science, Office of Biological and Environmental Research, Climate and Environmental Sciences Division. Additionally, a subset of data used in this article were produced as part of the international Multidisciplinary drifting Observatory for the Study of Arctic Climate (MOSAiC 2019–2020) supported by the RV Polarstern (AWI_PS122_00). The contribution of many people involved in collecting the MOSAiC data set and in all aspects of MOSAiC is acknowledged, as outlined in Nixdorf et al. (2021).

Funding

This research was supported, in part, by National Oceanic and Atmospheric Administration's Global Ocean Monitoring and Observing/Arctic Research Program and the U.S. Department of Energy Atmospheric Systems Research program projects DE-SC0022163, DE-SC0019251, and DE-SC0013306.

Competing interests

The authors have declared that no competing interests exist.

Author contributions

Conception and initial manuscript draft: SYM.

Participation in MOSAiC data acquisition: MDS, TU.

Analyses of the measurement data: SYM.

Scientific discussions and interpreting the data: SYM, MDS, TU.

Final approval of the version to be submitted: SYM, MDS, TU.

References

Bartholomew, M. 2020. Weighing bucket rain gauge instrument handbook. Available at https://www.arm.gov/publications/tech_reports/handbooks/doe-sc-arm-tr-232.pdf. Accessed 21 October 2020.

Battaglia, A, **Rustemeier, E**, **Tokay, A**, **Blahak, U**, **Simmer, C**. 2010. PARSIVEL snow observations: A critical assessment. *Journal of Atmospheric and Oceanic Technology* **27**: 333–344. DOI: http://dx.doi.org/10.1175/2009JTECHA1332.1.

Diamond, HJ, **Karl, TR**, **Palecki, MA**, **Baker, CB**, **Bell, JE**, **Leeper, RD**, **Easterling, DR**, **Lawrimore, JH**, **Meyers, TP**, **Helfert, MR**, **Goodge, G**. 2013. U.S. climate reference network after one decade of operations: Status and assessment. *Bulletin of the American Meteorological Society* **94**: 485–498. DOI: http://dx.doi.org/10.1175/BAMS-D-12-00170.1.

Falconi, MT, **von Lerber, A**, **Ori, D**, **Marzano, FS**, **Moisseev, D**. 2018. Snowfall retrieval at X, Ka and W bands: Consistency of backscattering and microphysical properties using BAECC ground-based measurements. *Atmospheric Measurement Techniques* **11**: 3059–3079. DOI: http://dx.doi.org/10.5194/amt-11-3059-2018.

Gaustad, K, **Riihimaki, L**, **Zhang, D**. 2019. MWR Retrievals (MWRRET1LILJCLOU). Atmospheric Radiation Measurement (ARM) user facility. DOI: http://dx.doi.org/10.5439/1027369.

Heymsfield, AJ, **Bansemer, A**, **Wood, NB**, **Liu, G**, **Tanelli, S**, **Sy, OO**, **Poellot, M**, **Liu, C**. 2018. Toward improving ice water content and snow-rate retrievals from radars. Part II: Results from three wavelength radar–-collocated in-situ measurements and CloudSat–GPM–TRMM radar data. *Journal of Applied Meteorology and Climatology* **57**: 365–389. DOI: http://dx.doi.org/10.1175/JAMC-D-17-0164.1.

Hodson, DLR, **Keeley, SPE**, **West, A**, **Ridley, J**, **Haekins, E**, **Hewitt, H**. 2013. Identifying uncertainties in Arctic climate change projections. *Climate Dynamics*

40: 2849–2865. DOI: http://dx.doi.org/10.1007/s00382-012-1512-z.

Huang, GJ, **Bringi, VN**, **Newman, AJ**, **Lee, G**, **Moisseev, D**, **Notaroš, BM**. 2019. Dual-wavelength radar technique development for snow rate estimation: A case study from GCPEx. *Atmospheric Measurement Techniques* **12**: 1409–1427. DOI: http://dx.doi.org/10.5194/amt-12-1409-2019.

Im, E, **Wu, C**, **Durden, SL**. 2005 May 9–12. Cloud profiling radar for the CloudSat mission. In *Proceeding IEEE Radar Conference*. Arlington, VA: 483–486. DOI: http://dx.doi.org/10.1109/RADAR.2005.1435874.

Kollias, P, **Treserras, BP**, **Protat, A**. 2019. Calibration of the 2007–2017 record of atmospheric radiation measurements cloud radar observations using CloudSat. *Atmospheric Measurement Techniques* **12**: 4949–4964. DOI: http://dx.doi.org/10.5194/amt-12-4949-2019.

Korolev, A, **Isaac, G**. 2003. Roundness and aspect ratio of particles in ice clouds. *Journal of the Atmospheric Sciences* **60**: 1795–1808. DOI: http://dx.doi.org/10.1175/1520-0469(2003)060<1795:RAAROP>2.0.CO;2.

Kropfli, RA, **Bartram BW**, **Matrosov, SY**. 1990. The upgraded WPL dual-polarization 8-mm Doppler radar for microphysical and climate research [Preprints]. *Conference on Cloud Physics*. San Francisco, CA: American Meteorological Society: 341–345.

Kulie, MS, **Bennartz, R**. 2009. Utilizing spaceborne radars to retrieve dry snowfall. *Journal of Applied Meteorology and Climatology* **48**: 2564–2580. DOI: http://dx.doi.org/10.1175/2009JAMC2193.1.

Kyrouac, J, **Holdridge, D**. 2019. Surface meteorological instrumentation (PWD). ARM mobile facility (MOS). Available at https://www.arm.gov/publications/tech_reports/handbooks/met_handbook.pdf. http://www.archive.arm.gov. Accessed 04 November 2020.

Kyrouac, J, **Springston, S**. 2019. *Meteorological Measurements associated with the Aerosol Observing System (AOSMET)*. Atmospheric Radiation Measurement (ARM) user facility. DOI: http://dx.doi.org/10.5439/1025153. Accessed 19 November 2020.

Lamb, HH, **Swenson, J**. 2005. Measurement errors using a Geonor weighing gauge with a Campbell Scientific datalogger [Extended abstract]. Available at https://ams.confex.com/ams/Annual2005/techprogram/paper_84196.htm. Accessed 21 October 2020.

Lindenmaier, I, **Johnson, K**, **Nelson, D**, **Isom, B**, **Hardin, J**, **Matthews, A**, **Wendler, T**, **Castro, V**. 2019. *Ka ARM Zenith Radar (KAZRCFRGE)*. Atmospheric Radiation Measurement (ARM) user facility. DOI: http://dx.doi.org/10.5439/1498936. Accessed 15 May 2021.

Maahn, M, **Hoffmann, F**, **Shupe, MD**, **de Boer, G**, **Matrosov, SY**, **Luke, EP**. 2019. Can liquid cloud microphysical processes be used for vertically pointing cloud radar calibration? *Atmospheric Measurement Techniques* **12**: 3151–3171. DOI: http://dx.doi.org/10.5194/amt-12-3151-2019.

Matrosov, SY. 2007. Modeling backscatter properties of snowfall at millimeter wavelengths. *Journal of the Atmospheric Sciences* **64**: 1727–1736. DOI: http://dx.doi.org/10.1175/JAS3904.1.

Matrosov, SY. 2019. Comparative evaluation of snowfall retrievals from the CloudSat W-band radar using ground-based weather radars. *Journal of Atmospheric and Oceanic Technology* **36**: 101–111. DOI: http://dx.doi.org/10.1175/JTECH-D-18-0069.1.

Matrosov, SY. 2021. Distinguishing between warm and stratiform rain using polarimetric radar measurements. *Remote Sensing* **13**(2): 214. DOI: http://dx.doi.org/10.3390/rs13020214.

Matrosov, SY, **Heymsfield, AJ**. 2017. Empirical relations between size parameters of ice hydrometeor populations and radar reflectivity. *Journal of Applied Meteorology and Climatology* **56**: 2479–2488. DOI: http://dx.doi.org/10.1175/JAMC-D-17-0076.1.

Matrosov, SY, **Mace, GG**, **Marchand, R**, **Shupe, MD**, **Hallar, AG**, **McCubbin, IA**. 2012. Observations of Ice crystal habits with a scanning polarimetric W-band radar at slant linear depolarization ratio mode. *Journal of Atmospheric and Oceanic Technology* **29**: 989–1008. DOI: http://dx.doi.org/10.1175/JTECH-D-11-00131.1.

Matrosov, SY, **Ryzhkov, AV**, **Maahn, M**, **de Boer, G**. 2020. Hydrometeor shape variability in snowfall as retrieved from polarimetric radar measurements. *Journal of Applied Meteorology and Climatology* **59**: 1503–1517. DOI: http://dx.doi.org/10.1175/JAMC-D-20-0052.1.

Matrosov, SY, **Shupe, MD**, **Djalalova, IV**. 2008. Snowfall retrievals using millimeter-wavelength cloud radars. *Journal of Applied Meteorology and Climatology* **47**: 769–777. DOI: http://dx.doi.org/10.1175/2007JAMC1768.1.

Matrosov, SY, Uttal, T, Shupe, MD. 2022. *Snowfall rate estimates using Ka-band radar measurements*. ARM Mobile Facility (MOS) MOSAiC (Drifting Obs - Study of Arctic Climate). DOI: https://dx.doi.org/10.5439/1853942.

Nemeth, K. 2008. OTT Pluvio2: Weighing Precipitation Gauge and Advances in Precipitation Measurement Technology. BDM Meteorology OTT MESSTECHNIK GmbH & Co. KG Ludwigstr. **16**, 87437. Kempten, Germany. Available at https://www.wmo.int/pages/prog/www/IMOP/publications/IOM-96_TECO-2008/P2(18)_Nemeth_Germany.pdf. Accessed 21 October 2020.

Nemeth, K, **Beck, E**. 2011. Precipitation measurement. *Meteorological Technology International Magazine* **2011**: 105–107.

Nixdorf, U, **Dethloff, K**, **Rex, M**, **Shupe, M**, **Sommerfeld, A**, **Perovich, DK**, **Nicolaus, M**, **Heuzé, C**, **Rabe, B**, **Loose, B**, **Damm, E**, **Gradinger, R**, **Fong, A**, **Maslowski, W**, **Rinke, A**, **Kwok, R**, **Spreen, G**, **Wendisch, M**, **Herber, A**, **Hirsekorn, M**, **Mohaupt, V**, **Frickenhaus, S**, **Immerz, A**, Weiss-**Tuider, K**,

König, B, **Mengedoht, D**, **Regnery, J**, **Gerchow, P**, **Ransby, D**, **Krumpen, T**, **Morgenstern, A**, **Haas, C**, **Kanzow, T**, **Rack, FR**, **Saitzev, V**, **Sokolov, V**, **Makarov, A**, **Schwarze, S**, **Wunderlich, T**, **Wurr, K**, **Boetius, A**. 2021. MOSAiC extended acknowledgement. DOI: http://dx.doi.org/10.5281/zenodo.5179738.

Pruppacher, HR, **Klett, JD**. 1978. *Microphysics of clouds and precipitation*. Dordrecht, Holland: D. Reidel: 714.

Rasmussen, R, **Baker B**, **Kochendorfer J**, **Meyers T**, **Landolt S**, **Fischer AP**, **Black J**, **Thériault JM**, **Kucera P**, **Gochis D**, **Smith C**. 2012. How well are we measuring snow: The OAA/FAA/NCAR winter precipitation test bed. *Bulletin of the American Meteorological Society* **93**: 811–829. DOI: http://dx.doi.org/10.1175/BAMS-D-11-00052.1.

Reinking, RF, **Matrosov, SY**, **Kropfli, RA**, **Bartram, BW**. 2002. Evaluation of a 45° slant quasi-linear radar polarization for distinguishing drizzle droplets, pristine ice crystals, and less regular ice particles. *Journal of Atmospheric and Oceanic Technology* **19**: 296–321. DOI: http://dx.doi.org/10.1175/1520-0426-19.3.296.

Shupe, MD, Rex, M, Blomquist, B, Persson, POG, Schmale, J, Uttal, T, Althausen, D, Angot, H, Archer, S, Bariteau, L, Beck, I, Bilberry, J, Bucci, S, Buck, C, Boyer, M, Brasseur, Z, Brooks, IM, Calmer, R, Cassano, J, Castro, V, Chu, D, Costa, D, Cox, CJ, Creamean, J, Crewell, S, Dahlke, S, Damm, E, de Boer, G, Deckelmann, H, Dethloff, K, Dütsch, M, Ebell, K, Ehrlich, A, Ellis, J, Engelmann, R, Fong, AA, Frey, MM, Gallagher, MR, Ganzeveld, L, Gradinger, R, Graeser, J, Greenamyer, V, Griesche, H, Griffiths, S, Hamilton, J, Heinemann, G, Helmig, D, Herber, A, Heuzé, C, Hofer, J, Houchens, T, Howard, D, Inoue, J, Jacobi, H-W, Jaiser, R, Jokinen, T, Jourdan, O, Jozef, G, King, W, Kirchgaessner, A, Klingebiel, M, Krassovski, M, Krumpen, T, Lampert, A, Landing, W, Laurila, T, Lawrence, D, Lonardi, M, Loose, B, Lüpkes, C, Maahn, M, Macke, A, Maslowski, W, Marsay, C, Maturilli, M, Mech, M, Morris, S, Moser, M, Nicolaus, M, Ortega, P, Osborn, J, Pätzold, F, Perovich, DK, Petäjä, T, Pilz, C, Pirazzini, R, Posman, K, Powers, H, Pratt, KA, Preußer, A, Quéléver, L, Radenz, M, Rabe, B, Rinke, A, Sachs, T, Schulz, A, Siebert, H, Silva, T, Solomon, A, Sommerfeld, A, Spreen, G, Stephens, M, Stohl, A, Svensson, G, Uin, J, Viegas, J, Voigt, C, von der Gathen, P, Wehner, B, Welker, JM, Wendisch, M, Werner, M, Xie, ZQ, Yue, F. 2022. Overview of the MOSAiC expedition: Atmosphere. *Elementa: Science of the Anthropocene* **10**: 1. DOI: http://dx.doi.org/10.1525/elementa.2021.00060.

Shupe, MD, **Rex, M**, **Dethloff, K**, **Damm, E**, **Fong, AA**, **Gradinger, R**, **Heuze, C**, **Loose, B**, **Makarov, A**, **Maslowski, W**, **Nicolaus, M**, **Perovich, D**, **Rabe, B**, **Rinke, A**, **Sokolov, A**, **Sommerfeld, A**. 2020. Arctic Report Card 2020: The MOSAiC expedition: A year drifting with the Arctic sea ice, in Thoman, RL, Richter-Menge, J, Druckenmiller, ML eds. Silver Springs, MD. DOI: http://dx.doi.org/10.25923/9g3v-xh92.

Souverijns N, **Gossart, A**, **Lhermitte, S**, **Gorodetskaya, IV**, **Kneifel, S**, **Maahn, M**, **Bliven, FL**, **van Lipzig, NPM**. 2017. Estimating radar reflectivity—Snowfall rate relationships and their uncertainties over Antarctica by combining disdrometer and radar observations. *Atmospheric Research* **196**: 211–223. DOI: http://dx.doi.org/10.1016/j.atmosres.2017.06.001.

Uttal, T, **Curry, JA**, **McPhee, MG**, **Perovich, DK**, **Moritz, RE**, **Maslanik, JA**, **Guest, PS**, **Stern, HL**, **Moore, JA**, **Turenne, R**, **Heiberg, A**, **Serreze, MC**, **Wylie, DP**, **Persson, OG**, **Paulson, CA**, **Halle, C**, **Morison, JH**, **Wheeler, PA**, **Makshtas, A**, **Welch, H**, **Shupe, MD**, **Intrieri, JM**, **Stamnes, K**, **Lindsay, RW**, **Pinkel, R**, **Pegau, WS**, **Stanton, TP**, **Grenfeld, TC**. 2002. Surface heat budget of the Arctic Ocean. *Bulletin of the American Meteorological Society* **83**: 255–276. DOI: http://dx.doi.org/10.1175/1520-0477(2002)083<0255:SHBOTA>2.3.CO;2.

Wagner, DN, Shupe, MD, Persson, OG, Uttal, T, Frey, MM, Kirchgaessner, A, Schneebeli, M, Jaggi, M, Macfarlane, AR, Itkin, P, Arndt, S, Hendricks, S, Krampe, D, Ricker, R, Regnery, J, Kolabutin, N, Shimanshuk, E, Oggier, M, Raphael, I, Lehning, M. 2021. Snowfall and snow accumulation processes during MOSAiC winter and spring season. *The Cryosphere Discuss* [preprint]. DOI: https://dx.doi.org/10.5194/tc-2021-126.

Wang, D, **Bartholomew, M**, **Shi, Y**. 2019. Atmospheric radiation measurement (ARM) user facility. ARM Mobile Facility (MOS) MOSAiC. Laser Disdrometer (LD). DOI: http://dx.doi.org/10.5439/1779709.

Webster, MA, **DuVivier, AK**, **Holland, MM**, **Bailey, DA**. 2020. Snow on Arctic Sea Ice in a warming climate as simulated in CESM. *Journal of Geophysical Research* **125**: e2020JC016308. DOI: http://dx.doi.org/10.1029/2020JC016308.

Wood, N, **L'Ecuyer, T**, **Vane, D**, **Stephens, G**, **Partain, P**. 2013. Level 2C snow profile process description and interface control document. Version 0, JPL Tech. Rep. 21 p. Available at http://www.cloudsat.cira.colostate.edu/sites/default/files/products/files/2C-SNOW-PROFILE_PDICD.P_R04.20130210.pdf.

How to cite this article: Matrosov, SY, Shupe, MD, Uttal, T. 2022. High temporal resolution estimates of Arctic snowfall rates emphasizing gauge and radar-based retrievals from the MOSAiC expedition. *Elementa: Science of the Anthropocene* 10(1). DOI: https://doi.org/10.1525/elementa.2021.00101

Domain Editor-in-Chief: Detlev Helmig, Boulder AIR LLC, Boulder, CO, USA

Guest Editor: Zoe Courville, U.S. Army Engineer Research and Development Center, Cold Regions Research and Engineering Laboratory, Hanover, NH, USA

Knowledge Domain: Atmospheric Science

Part of an Elementa Special Feature: The Multidisciplinary Drifting Observatory for the Study of Arctic Climate (MOSAiC)

Published: April 18, 2022 **Accepted:** March 15, 2022 **Submitted:** November 4, 2021

ELEMENTA Science of the Anthropocene

Elem Sci Anth is a peer-reviewed open access journal published by University of California Press.

OPEN ACCESS